Nat. Hazards Earth Syst. Sci. Discuss., 2, 2463–2529, 2014
www.nat-hazards-earth-syst-sci-discuss.net/2/2463/2014/
doi:10.5194/nhessd-2-2463-2014

Natural Hazards and Earth System Sciences
Open Access
Discussions

A multi-scale risk assessment for tephra fallout and airborne concentration from multiple Icelandic volcanoes – Part 1: Hazard assessment

S. Biass[1], C. Scaini[2], C. Bonadonna[1], A. Folch[2], K. Smith[3], and A. Höskuldsson[4]

[1]Section of Earth and Environmental Sciences, University of Geneva, Geneva, Switzerland
[2]CASE Department, Barcelona Supercomputing Center (BSC-CNS), Barcelona, Spain
[3]Geography, College of Life and Environmental Science, University of Exeter, Cornwall Campus, Penryn, UK
[4]Nordic Volcanological Center, University of Iceland, Reykjavík, Iceland

Received: 28 February 2014 – Accepted: 12 March 2014 – Published: 9 April 2014

Correspondence to: S. Biass (sebastien.biasse@unige.ch)

Published by Copernicus Publications on behalf of the European Geosciences Union.

Abstract

In order to assist the elaboration of proactive measures for the management of future volcanic eruptions in Iceland, we developed a new approach to assess the hazard associated with tephra dispersal and sedimentation at various scales and for multiple sources. The target volcanoes are Hekla, Katla, Eyjafjallajökull and Askja, selected either for their high probabilities of eruption and/or their high potential impacts. By coupling tephrostratigraphic studies, probabilistic techniques and modelling, we developed comprehensive eruption scenarios for both short and long lasting eruptions and compiled hazard maps for tephra ground deposition at a national scale and air concentration at a European scale using the TEPHRA2 and FALL3D models, respectively. New algorithms for the identification of realistic sets of eruptive source parameters are investigated, which assist the generation of probability density functions of eruption source parameters for the selected scenarios. Aggregation processes were accounted for using various empirical models. Outcomes help assessing and comparing hazard levels at different scales. For example, at a national scale Askja has a 5–10 % probability of blanketing the easternmost half of the country with a tephra accumulation of at least 1 kg m^{-2}. At a continental scale, Katla has a 5–10 % probability of producing ash clouds with concentrations of 2 mg m^{-3} over the UK, Scandinavia and northern Europe with a mean arrival time of 48–72 h and a mean persistence time of 6–18 h. In a companion paper, Scaini et al. (2014) present a vulnerability assessment for Iceland to ground deposition of tephra and for the European air traffic to airborne ash which, combined with the outcomes of the present paper, constitute one of the first multi-scale risk assessment associated with tephra dispersal and sedimentation.

NHESSD

2, 2463–2529, 2014

1 Introduction

Evaluation of the tephra hazard is necessary to carry out comprehensive risk assessments of explosive volcanoes. The process is commonly divided into a succession of logical steps, including the identification of eruptive sequences in the field, the development of comprehensive eruptive scenarios based on field observations and the use of models to quantify the hazard related to each eruptive scenario (Biass and Bonadonna, 2013; Biass et al., 2013; Bonadonna, 2006; Bonasia et al., 2011; Cioni et al., 2003; Connor et al., 2001; Costa et al., 2009, 2012; Jenkins et al., 2012a; Macedonio et al., 2008; Scaini et al., 2012; Volentik et al., 2009).

The hazard related to tephra dispersal is unique amongst volcanic threats. Although it rarely constitutes a direct threat to human lives, tephra can deposit on the ground up to 100's of km away from the source and be dispersed 1000's of km in the atmosphere, where its residence time can be as long as weeks. As a result, impacts from tephra vary with distance from the vent, resulting in complex vulnerability patterns of exposed elements (Blong, 1984; Connor et al., 2001). On the ground, tephra fallout can affect a wide range of aspects such as human health, buildings, lifelines, economy or the environment (see e.g. Table 1 in Biass and Bonadonna, 2013 for references). In the atmosphere, the presence of ash is able to paralyse air traffic far away from the source, revealing multiple vulnerable aspects of modern societies (Budd et al., 2013; Davies et al., 2010; Swindles et al., 2011; Wilkinson et al., 2012), as demonstrated by the 2010 Eyjafjallajökull and the 2011 Puyehue–Cordón Caulle eruptions. Nonetheless, probabilistic studies of tephra dispersal tend to focus either on local ground deposition (e.g. Biass and Bonadonna, 2013) or on far-range atmospheric concentrations (e.g. Sulpizio et al., 2012), and only a few recent studies account for comprehensive multi-scale assessments (e.g. Scaini et al., 2012).

One crucial parameter for the description of the dispersal of tephra is the total grainsize distribution (TGSD), which typically varies within several orders of magnitude for a given eruption. Centimetric to millimetric particles are controlled by gravitational

NHESSD
2, 2463–2529, 2014

settling and sediment in proximal to medial distances from the eruptive vent, whereas micrometric to sub-micrometric particles are controlled by larger-scale atmospheric processes and transported at continental scales (Folch, 2012). Depending on the assumptions used to model these two end-members, several modelling approaches have been developed to solve the advection–diffusion equation either in analytical, semi-analytical or numerical ways (Bonadonna et al., 2012; Folch, 2012).

Eruption scenarios are usually developed for a single volcano and are constrained by the availability of past data and the completeness of the eruptive record (Marzocchi et al., 2004). Through time, the definition of eruption scenarios has evolved from a "worst-case scenario" approach towards an evaluation of the entire range of activity at a given volcano. For example, early hazard maps for Cotopaxi volcano (Hall and Hillebrandt, 1988; Vink, 1984) are based upon isopach maps of two major eruptions with opposite wind directions in agreement with the regional wind patterns and the most important exposed human settlements. More recent studies considered a probabilistic approach and developed a set of eruptive scenarios of various intensities based on precise stratigraphic studies (Biass and Bonadonna, 2011, 2013). Probabilistic techniques such as Monte-Carlo simulations (e.g. Hurst and Smith, 2004) are nowadays an integrant part of any hazard assessment for tephra dispersal and are used to investigate both the missing or inaccessible parts of the geological record and the impacts of eruptions in a representative set of atmospheric conditions (Bonadonna, 2006).

For probabilistic modelling, the identification of eruption scenarios typically requires the definition of a probability density function (PDF) for each input parameter needed by a given model in order to account for the variability of eruptive processes (i.e. aleatoric uncertainty). For tephra fallout, several approaches have been used to define eruption scenarios, based either on individual eruptions (Bonasia et al., 2011; Capra et al., 2008), eruptive styles (Macedonio et al., 2008), intensities/magnitudes (Scaini et al., 2012; Yu et al., 2013) or VEI classes (Biass and Bonadonna, 2013), mostly applied to a single source. However, some regions in the world are under the threat

NHESSD
2, 2463–2529, 2014

of more than one volcano, sometimes presenting a wide range of known eruptive styles and characteristics, and the development of comparable eruption scenarios for a set of volcanoes becomes an obvious necessity. Examples of multi-volcano hazard assessments include the works of Jenkins et al. (2012a, b) that assess the tephra hazard for the Asia-Pacific region considering eruptions of VEI greater or equal to 4 from 190 volcanoes with eruptive scenarios based on the Global Volcanism Program (Simkin and Siebert, 1994). Ewert (2007) uses the relative threat to human settlements as an indicator to rank 169 US volcanoes and Hurst and Smith (2004) produced a probabilistic assessment of tephra accumulation for the North Island of New Zealand considering three volcanoes, and basing their eruption scenarios mainly on analogue eruptions. More recently, Lirer et al. (2010) have produced a multi-source hazard assessment of the Campanian region considering tephra fall and pyroclastic flows from three volcanoes, based on the compilation of all field studies present in the literature.

Here, we present a medium- to long-term multi-scale hazard assessment for ground tephra accumulation and far-range atmospheric ash dispersal from four Icelandic volcanoes – Hekla, Katla, Askja, and Eyjafjallajökull – selected either for their high probabilities of eruption in the near future or their high potential impact (Fig. 1). Due to the different eruptive styles and the varying degree of knowledge of the eruptive history at these volcanoes, we developed consistent probabilistic eruption scenarios based on field data, literature studies and historical reports. The tephra-related hazard was assessed for each eruption scenario at a local scale (i.e. ground tephra accumulation) with the analytical model TEPHRA2 (Bonadonna et al., 2005) and at a regional scale (i.e. atmospheric concentration) with the numerical model FALL3D (Costa et al., 2006; Folch et al., 2009). A population of 10 years of wind inferred from reanalysis datasets was used to assess statistical atmospheric conditions. Outputs include (i) probabilistic maps of ground tephra accumulation and atmospheric concentration for relevant thresholds, (ii) mean atmospheric travel time and persistence time (i.e. time during which concentrations exceed a given threshold), (iii) probability maps of atmospheric travel time and persistence time for relevant thresholds, and (iv) ground

NHESSD
2, 2463–2529, 2014

hazard curves for critical facilities in Iceland. In a companion paper, Scaini et al. (2014) present a vulnerability assessment for both Iceland and the European air traffic system and use the outcomes of this study to perform a multi-scale impact analysis. This comprehensive assessment aims at serving as a starting point for the elaboration of pro-active measures for the management of explosive volcanic crisis.

2 Geological setting

Iceland is the result of the combined effects of a spreading plate boundary and a mantle plume (Allen et al., 1999; Vink, 1984; White et al., 1995; Wolfe et al., 1997). Current active volcanic zones (i.e. the neovolcanic zones) are the superficial expression of the mid-oceanic ridge. Arranged as discrete 15–50 km-wide belts of active faulting and volcanism, they collectively cover a total area of 30 000 km^2 (Gudmundsson, 2000; Thordarson and Höskuldsson, 2008; Thordarson and Larsen, 2007). Volcanic zones host volcanic systems which, in their simplest forms, contain either a fissure swarm, a central volcano or both (Gudmundsson, 1995a, b). When present, the central volcano is the focal point of eruptive activity and the largest edifice in each system under which crustal magma chambers can develop, giving rise to either silicic or basaltic magmatism. On the contrary, only basaltic magmas are erupted within fissure swarms (Larsen and Eirìksson, 2008; Thordarson and Larsen, 2007).

2.1 Target volcanoes

In this paper, we focus on eruptions occurring at the central volcano of four different volcanic systems, located within two different volcanic zones: the Eastern Volcanic Zone (EVZ) and the Northern Volcanic Zone (NVZ; Fig. 1), ranked first and third in terms of volcanic activity throughout the Holocene (Thordarson and Höskuldsson, 2008). No volcanic system was considered within the second most active volcanic zone, the Western Volcanic Zone (WVS), because the EVZ is an active axial rift

NHESSD
2, 2463–2529, 2014

propagating southwards, thus taking over the activity of the WVS (Mattsson and Höskuldsson, 2003; Thordarson and Larsen, 2007). The EVZ is divided into two sectors. In the north, the axial rift zone is characterized by a thick crust, high heat flow, well-developed tensional features and the production of tholeitic basalts. The southern propagating tip of the EVZ is often referred as a flank zone, which lies on an older and thinner crust presenting a lower heat flow. Here, tensional features are poorly developed and the magma production consists mainly of transitional alkali to alkali basalts (Loughlin, 2002; Mattsson and Höskuldsson, 2003). Here we consider three volcanoes from the EVZ (Hekla, Katla, and Eyjafjallajökull; Fig. 1) and one from the NVZ (Askja).

2.1.1 Hekla

Hekla volcano is located on the southwest extremity of the EVZ and is one of the most active volcanic systems in Iceland, with 18 eruptions from the central vent and 6 in its vicinity since human settlement in Iceland during the last 1100 years (Table 1). The average recurrence rate of eruptions at Hekla was one to two per century until the 1970's, when the regime drastically changed to a regular 10-year repose time with eruptions in 1970, 1980–1981, 1991, and 2000. Since the first historical eruption in 1104, which followed a period of quiescence of 250 years, repose intervals have varied between 10 and 102 years. Interestingly, the repose interval has been recognized as having a strong influence on the magma composition of the following eruption, with a silica content increasing with the length of the interval (Gronvold et al., 1983; Gudmundsson et al., 1992; Höskuldsson et al., 2007; Thorarinsson, 1967). Although voluminous Plinian explosive deposits from pre-historic eruptions of Hekla are recognized in the field (e.g. H1–5 layers; Larsen and Eirìksson, 2008), this study focuses on the eruptive behaviour through historical times, known as "mixed" (Thordarson and Höskuldsson, 2008; Thordarson and Larsen, 2007). Most eruptions are described as being long-lasting (i.e. week to months) including both explosive and effusive activity scattered over three main phases, where the tephra/lava ratio

NHESSD
2, 2463–2529, 2014

decreases with time. In the first phase, a sub-plinian to Plinian-type plume typically develops few minutes after the onset of the eruption and lasts for about 1 h. The second phase is a several-hour long transition phase with moderate tephra production and lava fountaining leading to the last phase, characterized by a discrete weeks to months-long Strombolian activity (Thordarson and Höskuldsson, 2008). Here, we model only the first phase known for producing the majority of the tephra.

Based on stratigraphic investigations and reviews of historical reports, Thorarinsson (1967) identified 14 eruptions since the settlement of Iceland (870s AD, Vésteinsson, 2000) until the eruption of 1947, with major tephra emissions in 1140, 1300, 1510, 1597, 1693, 1766, and 1845. These eruptions, along with the eruption of 1947, show strong similarities in terms of isopach maps, eruptive styles and erupted volumes. Precise eyewitness reports and field studies exist for the eruptions of 1947, 1970, 1980–1981, 1991, and 2000. It is clear that the volume produced by the 1947 eruption is larger than that associated with the following eruptions, which exhibit similar volumes and deposition trends (Gronvold et al., 1983; Gudmundsson et al., 1992; Höskuldsson et al., 2007; Thorarinsson, 1967; Thorarinsson and Sigvaldason, 1972).

2.1.2 Katla

The Katla volcanic system lies on the south-eastern sector of the flank zone of the EVZ, at the transition of divergent plate motion (Sturkell et al., 2010). It is composed by a central volcano and an embryonic fissure swarm, about 110 km long with a 100 km^2 caldera in the centre of the edifice and covered by the 590 km^2 and up to 700 m thick Mýrdalsjökull ice cap (Björnsson et al., 2000; Óladóttir et al., 2008). Three types of eruptive styles are known to have occurred at Katla, which include basaltic explosive eruptions (most typical), silicic explosive eruptions and long-lasting effusive eruptions such as the Eldgjá eruption of 934–940, which curbed the settlement in Iceland (Larsen, 2000). Up to 208 tephra layers are recognized as originating from Katla during the past 8400 years, amongst which 18 were witnessed during historical times (Larsen, 2000, 2010; Larsen and Eirìksson, 2008; Larsen et al., 2001; Thordarson

NHESSD
2, 2463–2529, 2014

and Larsen, 2007). Óladóttir et al. (2008) observe two cycles during the Holocene, each involving three plumbing system stages. From 6600 to 1700 BP, 12 moderate-size silicic eruptions of dacitic composition took place at Katla, known as the SILK layers (Larsen et al., 2001). In terms of volumes of eruption frequency, Katla is the most productive volcanic system in Iceland (Larsen and Eirìksson, 2008; Óladóttir et al., 2006; Thordarson and Larsen, 2007). The eruption frequency at Katla is about two eruptions per century since 1500 AD, with a mean repose interval of 47 years (Larsen, 2000). However, due to the preferential conservation of the deposits in the East sector of the volcano related to the presence of an ice cap and a current period of low activity, this estimate can potentially be twice as much throughout the entire Holocene (Óladóttir et al., 2008, 2006). Interestingly, the duration of the repose interval can be correlated with the size of the preceding eruption, where large eruptions lead to long reposes (Eliasson et al., 2006).

Ten eruptions were reported since 1580 AD, all located within the caldera and began during the May–November period (Larsen, 2000, 2010; Thordarson and Larsen, 2007; Table 2). The last tephra-producing eruption occurred in 1918, generating a plume rising up to 14 km a.s.l. and a total erupted volume ranging between 0.7 and 1.5 km^3 (Larsen, 2010). Throughout historic time, erupted volumes of freshly fallen tephra have ranged between 0.02 and 1.5 km^3. The largest of these volumes was produced by the K-1755 eruption, which heavily impacted farming activities and caused 50 farms to be abandoned (Larsen, 2000, 2010). Since 1625, eruptions are documented to have lasted from 2 weeks to 5 months, with 80–90 % of total tephra generated during the first few days (Larsen, 2010). Since 1918, three crises occurred at Katla in 1955, 1999–2004, and 2011 accompanied with the generation of jökulhaups and high seismic activity (Soosalu et al., 2006; Sturkell et al., 2010). These crises have been suggested to represent either shallow magma intrusions or small sub-glacial eruptions. Discarding these crises as eruptions, the repose interval since the last eruption is 94 years, which results in a > 20 % probability of eruption in the next 10 years (Eliasson et al., 2006).

NHESSD
2, 2463–2529, 2014

2.1.3 Eyjafjallajökull

Eyjafjallajökull is located in the central southern part of the EVZ, within the transitional flank zone. The 1651 m high edifice covers a surface of 400 km^2 and is capped by a 200 m thick ice cap (Loughlin, 2002; Sturkell et al., 2010). The pre-17th century eruptive history is poorly known, with the knowledge of two eruptions during the 6–7th century and again in 920 AD (Dugmore et al., 2013). Only three eruptions are reported during historical times, namely in 1612, 1821–1823, and 2010 (Gudmundsson et al., 2010; Sturkell et al., 2010). All eruptions are considered to be similar in composition and magnitudes, i.e., VEI 3–4 (Gudmundsson et al., 2010).

The long-lasting and pulsating eruption of 2010 started on 20 March, following a period of almost 20 years of unrest marked by intrusion-related deformation and seismic crisis in 1994 and 1999 (Gudmundsson et al., 2010; Sigmundsson et al., 2010; Sturkell et al., 2010). The first phase was characterized by a 3-week long basaltic effusive eruption from a flank vent located east of the summit, between the Katla and Eyjafjallajökull volcanoes. Once the activity on the flank vent ceased (around 12 April), the activity resumed at the central summit vent on 14 April with moderate explosive to effusive activity. The activity of the summit vent can be divided into three phases based on variation in the eruptive styles. During explosive phases, the plume oscillated between 1 and 10 km a.s.l. (Arason et al., 2011; Gudmundsson et al., 2010). The total volume of tephra produced is 0.27 km^3, of which 80 % was airborne and the remaining 20 % was transported by ice and water (Gudmundsson et al., 2012). A precise chronology of the eruption can be found in the works of Arason et al. (2011), Bonadonna et al. (2011) and Gudmundsson et al. (2012).

2.1.4 Askja

Askja volcano lies on the southern part of the NVZ, of which it is the largest central volcano (Sparks et al., 1981). Askja volcanic system is composed by a central volcano and a swarm of fissures, faults and crater rows extending 120 km north towards the

NHESSD
2, 2463–2529, 2014

coast and 30 km south towards Vatnajökull glacier (Hjartardóttir et al., 2009). During historic time, eruptions have occurred both within fissures and the central volcano. The fissure swarm eruptions are all basaltic and effusive, while the central volcano ones are both of the effusive basaltic style as well as rhyolitic and explosive. The most recent activity phase of this volcanic system began in September 1874 and lasted until 1961 with a total of 9 eruptions in 1875, of which one rhyolitic and explosive. During the 20th century a total of 8 eruption have occurred at the volcano, 7 within the central volcano and on south of it (Hartley and Thordarson, 2012; Sparks et al., 1981). The most recent explosive eruption was a VEI 5 rhyolitic Plinian eruption, which began on 28 March 1875 and lasted for about 17 h (Hartley and Thordarson, 2012; Sparks et al., 1981). More than 95 % of the total volume of tephra (i.e. about 2 km^3) was produced during the phases Askja C and Askja D, separated by a 30 min break. Askja C is related to a phreatoplinian activity and is the only historical example of this eruptive style (Carey et al., 2010). It lasted for 1–1.5 h, produced a plume reaching an altitude of 23 km and a volume of 0.45 km^3 of tephra composed of 99 wt.% of particles smaller than 1 mm (Carey et al., 2010; Sparks et al., 1981). The following phase, Askja D, was a dry Plinian eruption which lasted for 4–6 h, produced a plume reaching an altitude of 26 km and a volume of tephra close to 1.37 km^3 (Carey et al., 2010; Sparks et al., 1981). In addition to the 1875 eruption, evidence for another large rhyolitic eruption from Askja dating back to about 10 ka can be observed within the Askja central volcano and along the NE coast of Iceland (Sigvaldason, 2002). The volume of tephra for this event is estimated to be around 5–10 km^3 (Larsen and Eirìksson, 2008).

3 Method

Here, we aim to assess the hazard caused by the ground deposition and the atmospheric dispersion of tephra. Probabilistic approaches are adopted in order to account for the variability (i.e. aleatoric uncertainty) related to both atmospheric

NHESSD
2, 2463–2529, 2014

conditions and eruption types. For ground accumulation, we quantify:

$$P\left[M(x,y) \geq M_{\mathrm{T}} | \text{eruption}\right] \tag{1}$$

where $M(x,y)$ is the tephra load ($\mathrm{kg\,m^{-2}}$) accumulated at a given location and M_{T} a load threshold (e.g. Bonadonna, 2006). For a given eruption scenario, the probability P_{M} at a pixel (x,y) is quantified by counting the number of times a given threshold of load is reached over the total number of runs N:

$$P_{\mathrm{M}}(x,y) = \frac{\sum_{i=1}^{N} n_i}{N} \tag{2}$$

where

$$n_i(x,y) = \begin{cases} 1 & \text{if } M_i(x,y) \geq M_{\mathrm{T}} | \text{eruption} \\ 0 & \text{otherwise} \end{cases} \tag{3}$$

For atmospheric concentrations, we start by quantifying:

$$P\left[C(x,y,z,t) \geq C_{\mathrm{T}} | \text{eruption}\right] \tag{4}$$

where $C(x,y,z,t)$ is the tephra mass concentration in the atmosphere ($\mathrm{mg\,m^{-3}}$) at a given point and time instant and C_{T} a mass concentration threshold. For a given eruption scenario, the probability of disruption P_{C} at a point (x,y,z) is quantified by counting the number of times a given mass concentration threshold is exceeded over the total number of runs N:

$$P_{\mathrm{C}}(x,y,z) = \frac{\sum_{i=1}^{N} n_i}{N} \tag{5}$$

where

$$n_i(x,y,z) = \begin{cases} 1 & \text{if } \exists t \text{ such that } C_i(x,y,z) \geq C_{\mathrm{T}} | \text{eruption} \\ 0 & \text{otherwise} \end{cases} \tag{6}$$

NHESSD
2, 2463–2529, 2014

Disruption can be calculated at a given height or Flight Level (FL) or be comprehensive of all FLs, that is, considering that disruption occurs at a point (x, y) if the critical condition is achieved at any height or FL above the point. In any case, note that for a given run, disruption occurs regardless of the number of time slabs during which Eq. (6) is verified. For this reason, and in order to assess the degree of disruption to the aviation sector, we also compute the mean persistence (i.e. the duration of a disruption). Persistence is calculated counting, for each run, the number of time slabs in which the critical threshold is exceeded. The mean persistence time results from averaging persistence over the total number of runs. Again, this can be done for a specific FL (height) or considering all the vertical levels simultaneously. Finally, another parameter of interest to Air Traffic Management (ATM) is the arrival time, defined as the time from the beginning of the eruption to the beginning of the first slab of disruption at the considered height (or at any level in the case of the comprehensive assessment). The mean arrival time results from averaging arrival times of single runs over the total number of runs. For both persistence and arrival time, we also computed the standard deviation over the total number of runs and the probabilities of exceeding relevant thresholds of persistence and arrival times following the same approach as Eq. (5).

Given that the management of airspace is nowadays conditioned by airspace closure/opening and that airspaces include many FLs, a map comprehensive of all FLs can better support ATM. Note that the simultaneous analysis of all FLs produces more conservative results, giving a larger probability of disruption, a larger persistence (because disruption at different FLs can occur at non-overlapping time slaps) and lower arrival time.

In this section, we review (i) the models used at different scales, (ii) the probabilistic strategies adopted in this study, and (iii) the strategy used to account for particle aggregation processes.

NHESSD
2, 2463–2529, 2014

3.1 Tephra modelling

3.1.1 Ground accumulation

The hazard related to ground deposition of tephra was assessed at the scale of Iceland using the steady semi-analytical advection–diffusion model TEPHRA2 (Bonadonna et al., 2005) following the approach detailed in Biass and Bonadonna (2013). TEPHRA2 requires five main input parameters: plume height, eruption duration, erupted mass, total grainsize distribution (TGSD) and particle density. It also requires a vertical wind profile, a calculation grid and three empirical parameters: a fall-time threshold acting as a threshold for the modelling of the diffusion of small and large particles (i.e. power law vs. linear diffusions), a diffusion coefficient used for the linear diffusion law and an apparent eddy diffusivity fixed at $0.04\,m^2\,s^{-1}$ for the power-law diffusion (Bonadonna et al., 2005; Suzuki, 1983; Volentik et al., 2009). Empirical parameters can be estimated either using TEPHRA2 in inversion mode when enough field data are available (Connor and Connor, 2006; Volentik et al., 2009) or using analogue eruptions. Wind conditions for the 2001–2010 period were extracted from the NOAA NCEP/NCAR Reanalysis dataset (Kalnay et al., 1996) at a 2.5° resolution, providing 4-daily wind profiles. Finally, the calculation grid covers the small computational domain (Fig. 1) at a resolution of 1 km. When needed, smaller calculation grids were used at a resolution of 500 m.

3.1.2 Atmospheric concentration

The hazard related to the atmospheric dispersal of tephra was assessed at the continental scale using the non-steady numerical advection–diffusion-sedimentation model FALL3D (Costa et al., 2006; Folch et al., 2009). Following the approach of Scaini et al. (2012), we applied probabilistic techniques commonly used with analytical models to produce long-term hazard maps for ash dispersal (Folch and Sulpizio, 2010; Scaini et al., 2012; Sulpizio et al., 2012). Eruption Source Parameters (ESP) required

NHESSD
2, 2463–2529, 2014

by FALL3D include plume height, mass eruption rate (MER), eruption date and eruption duration. Following Folch et al. (2009), horizontal and vertical diffusion coefficients are fixed to 5000 and 100 $m^2 s^{-1}$, respectively. Models for vertical mass distribution and terminal velocity of tephra particles are those of Suzuki (1983) and Ganser (1993), respectively. Meteorological fields for the considered period were extracted from the ECMWF Era-Interim Reanalysis at 1.5° and the computational domain covers northern and central Europe (Fig. 1). In order to reduce the computational cost related to a probabilistic application of FALL3D, the stratified sampling technique was applied for the stochastic sampling of both wind profiles and ESP, allowing to achieve a similar sampling accuracy as a PDF with much less members (Costa et al., 2009; Rao and Krishnaiah, 1994; Scaini et al., 2012).

3.2 Probabilistic strategies

Several approaches exist to assess the probability distribution of reaching a hazardous accumulation of tephra given an eruption (Bonadonna, 2006). In order to account for variable parameters (i.e. eruptive and atmospheric conditions), a large number of model runs are performed varying input parameters, including eruption date (i.e. wind profile for TEPHRA or 4D variables for FALL3D). Each run consists either of a single occurrence of the model (i.e. short-lasting eruptions) or a set of simulations in time (i.e. long-lasting eruptions). When an approach with variable eruptive parameters is adopted, a PDF must be defined to constrain the stochastic sampling. The definition of the PDF, which reflects the knowledge of the system, is relevant to the definition of eruptive scenarios and will be tackled later.

NHESSD
2, 2463–2529, 2014

3.2.1 Short-lasting eruptions

One Eruption Scenario (OES)

The OES is an approach used to compile the probability of reaching a given threshold of tephra accumulation in variable wind conditions, with ESP chosen deterministically. Figure 2a summarizes the algorithm applied to short-lasting eruptions (Bonadonna, 2006). First, the plume height, the eruption duration, the total mass and the TGSD are fixed deterministically. Then, for each single run of the model, an eruption date is sampled from which the corresponding wind profile is extracted from the meteorological database.

Eruption Range Scenario (ERS)

In addition to varying wind conditions, the ERS approach allows for a stochastic sampling of ESP at each run (Bonadonna, 2006). Each variable parameter (typically the plume height, erupted mass/duration/mass eruption rate and the TGSD) is characterized by a range and a PDF. Figure 2b shows the algorithm used for the ERS. First, a plume height, an eruption duration and an eruption date are sampled from their respective PDF, and a mass boundary for the eruption scenario is set. From the eruption date, the respective meteorological conditions are loaded, which in turn, combined with the plume height, allows for the calculation of the MER using the method of Degruyter and Bonadonna (2012) fixing the height of the tropopause to 10 km a.s.l. (Lacasse, 2001). A test is then performed to assess whether the resulting mass, calculated by combining the MER and the eruption duration, fits into the initial assumptions of mass range. If the test is negative, all parameters are resampled, otherwise the selected input parameters are sent to the model.

NHESSD
2, 2463–2529, 2014

3.2.2 Long-lasting eruptions

In order to assess the hazard related to long-lasting eruptions, we developed new eruption scenarios with algorithms summarized in Fig. 2c and d. When long-lasting eruptions are tackled, ESP are expressed as time-series at constant time intervals, Δt, defined depending on the availability of data (i.e. measurements of plume height, wind profiles). The application of algorithms shown in Fig. 2c and d varies depending on the scale of the hazard assessment, and thus the model used. When used with steady models (e.g. TEPHRA2), they consist of discrete model runs at constant time intervals, and the final hazard maps are the sum of all individual runs (e.g. Scollo et al., 2013). When used with non-steady models (e.g. FALL3D), ESP (i.e. plume height, MER) are updated at a constant time interval. For clarity, we will refer to any single run or update of the model as "occurrence", i.e., for long-lasting eruptions, a run (i loop in Fig. 2) consists of several occurrences (j loop in Fig. 2).

Long-Lasting One Eruption Scenario (LLOES)

The LLOES relies on the same concept as the OES, i.e. eruptive parameters chosen deterministically with varying wind conditions, only applied to long-lasting eruptions. Here, the total eruption duration, the time-series of plume heights and the TGSD are set deterministically, and the time interval (Δt) is set based on the availability of data. At each run of the model, an eruption date is sampled and the corresponding wind profiles are extracted based on the eruption duration and Δt. At each occurrence, knowing Δt, the plume height and the wind conditions at the given time, the MER and the mass are calculated averaged over the interval length, and a new occurrence of the model is performed. Each run is the sum of all occurrences performed.

NHESSD
2, 2463–2529, 2014

Long-Lasting Eruption Range Scenario (LLERS)

The LLERS applies the ERS strategy to long-lasting eruptions. Eruptive parameters are stochastically sampled as time-series at a constant Δt. Following the algorithm in Fig. 2d, a mass boundary is first set. At each run, an eruption date and an eruption duration are sampled. At each occurrence, a plume height is sampled from a PDF, and the MER is calculated based on the wind conditions for that specific date using the method of Degruyter and Bonadonna (2012). If the sum of the mass of all occurrences of a single run falls out of the initial mass assumptions, the sampling process is restarted. If not, input values for all occurrences are sent to the model. Eventually, each run is the sum of all occurrences performed.

3.3 Ash aggregation

Aggregation processes are known to modify deposition trends along the dispersal axis by aggregating fine particles (typically < 100 µm) into larger clusters (Bonadonna et al., 2002; Brown et al., 2012; Rose and Durant, 2011). The fallout of aggregates has been observed during numerous eruptions, including the 1980 eruption of Mount St. Helens (Carey and Sigurdsson, 1982), the on-going eruption of Montserrat (Bonadonna et al., 2002) and the 2010 eruption of Eyjafjallajökull (Bonadonna et al., 2011; Taddeucci et al., 2011). Although aggregation is a topic of intense research, no satisfactory parameterization of this process has been achieved yet (Bagheri et al., 2013; Costa et al., 2010; Folch et al., 2010; Van Eaton and Wilson, 2013; Van Eaton et al., 2012). The aggregation of fine particles into larger aggregates results in premature sedimentation in the proximal area and in a relative depletion of fines away from the vent (Carey and Sigurdsson, 1982; Hildreth and Drake, 1992). Ignoring aggregation would result in an underestimation of the hazard in proximal areas and an overestimation in distal sectors.

Several models attempt to describe aggregation processes using either empirical (Bonadonna and Phillips, 2003; Carey and Sigurdsson, 1982; Cornell et al., 1983)

NHESSD
2, 2463–2529, 2014

or numerical approaches (Costa et al., 2010; Folch et al., 2010). Here, we use the empirical observations from Bonadonna et al. (2002) and Bonadonna et al. (2011) to modify the TGSD before running the models. Following this approach, we remove an equal proportion of masses of fine particles from phi classes $\geq 4\Phi$, which are equally re-distributed between classes -1Φ and 3Φ. The amount of fine particles removed, i.e. the aggregation coefficient, is stochastically sampled between 20 and 80 % on a uniform distribution at every loop increment on the algorithms shown in Fig. 2.

4 Results

4.1 Identification of eruption scenarios

The identification of eruption scenarios is based on the eruption history presented in Sect. 2.1 for each volcano. Since no explosive eruptions are recognised as originating from fissure swarms, we only focus on activity occurring at the central vent of the selected volcanic systems. For the assessment of tephra ground accumulation, each eruption scenario consists of 1000 runs of the model of TEPHRA2. In order to reduce the computational cost related to the probabilistic application of FALL3D, the sampling technique proposed by Scaini et al. (2012) was applied, allowing to achieve a similar sampling accuracy with almost one order of magnitude less members. Since neither monthly nor seasonal trends are shown by the statistical analysis of wind profiles, we used a population of 10 years of wind data (2001–2010). Figure 3 shows wind roses at three altitude levels for points specified in Fig. 1.

4.1.1 Hekla

Out of all volcanoes considered in this study, Hekla presents the most accurate historic record with 18 identified and reasonably well-described eruptions and a good characterization of 5 of them and a TGSD of the 2000 eruption (Gronvold et al., 1983; Gudmundsson et al., 1992; Höskuldsson et al., 2007; Smith et al., 2014; Thorarinsson,

NHESSD
2, 2463–2529, 2014

1967; Thorarinsson and Sigvaldason, 1972). From the 18 eruptions presented in Table 1, we discarded the eruption of 1104 from the eruptive record as it belongs to the larger magnitude and lower frequency H1–5 series and occurred after a repose interval of > 230 years, more than twice the maximum repose time in historical times (Larsen and Eirìksson, 2008; Thordarson and Höskuldsson, 2008; Thordarson and Larsen, 2007). As mentioned in Sect. 2.1.1, historical eruptions at Hekla are classified as "mixed". Since a large majority of the tephra is produced during the opening phase, we only model the first part of the eruption.

Based on the historical period summarized in Table 1, two eruption scenarios were identified for Hekla and named after the best-described eruption of each cluster. First, a 2000-type eruption was identified to describe eruptions that have occurred at a ∼10 years frequency. This eruption scenario considers all available data for the eruptions of 1222, 1970, 1981, 1991 and 2000. Second, a 1947-type eruption is considered representative of larger Plinian eruptions occurring on an average of one per century starting from the eruption of 1158 (Thorarinsson, 1967).

2000-type scenario

The good knowledge of eruptions considered in the 2000-type scenario allows for the identification of well-constrained ranges of ESP for plume heights and erupted masses, and, subsequently, the use of the ERS strategies. Table 3 and Fig. 4 summarize ranges of ESPs and their corresponding PDFs. In agreement with historical witnesses, the duration of the intense opening phase was fixed between 0.5 and 1 h and sampled on a uniform PDF. Based on Table 1 and following the algorithm presented in Fig. 2, a mass constraint was fixed between 6.9×10^9 and 6.9×10^{10} kg considering a deposit density of 691 kg m^{-3} (Smith et al., 2014). Based on observations, plume heights were defined between 6 and 16 km a.s.l. and sampled on a logarithmic scale in order to slightly favour small events over large ones. As described in Sect. 3.2.2, the mass is calculated as a combination of the plume height and the eruption duration. Therefore, the algorithm shown in Fig. 2 constrains the sampling of both plume height

NHESSD
2, 2463–2529, 2014

and eruption duration in order to obtain only plausible sets of ESP consistent with the initial assumptions on the erupted mass. As a result, although the stochastic sampling of plume heights is constrained on a logarithmic PDF, the resulting distribution shown in Fig. 4a is truncated towards the lowest boundary of our initial assumptions, suggesting the incompatibility of these values of plume heights to produce the expected masses. This distribution of plume heights obtained for the 2000-type eruption results in a logarithmic distribution of masses (Fig. 4b).

The TGSD for the 2000 eruption is available from Smith et al. (2014), which shows bimodality with peaks at −3Φ and 3Φ (Fig. 4c) and a minimum at 1Φ. This TGSD was used as representative for the 2000-type eruption scenario and was varied at each run. First, considering 1Φ as a boundary between the two populations, we varied the relative weight percentage of the two populations between 30 and 70 %. Second, we applied the aggregation model described in Sect. 3.3 on the resulting modified TGSD by removing between 20 and 80 % of fines. Figure 4c shows the three states of the TGSD for one of the 1000 runs.

1947-type scenario

A similar approach was applied to the 1947-type scenario. Since only sparse estimates of plume heights are reported in the literature for this eruption type, the sampling was constrained between 16 (i.e. the highest boundary of the 2000-type eruption) and 30 km a.s.l. on a logarithmic PDF (Fig. 4d). Based on Table 1, the mass constraint was defined between 6.9×10^{10} and 3.5×10^{11} kg (Fig. 4e). The resulting distribution of plume heights is shown in Fig. 4d and displays a maximum of sampling around 18–20 km a.s.l. No solution compatible with the mass constraint was found for plumes higher than 27 km. Figure 4e shows a rather uniform mass distribution, though slightly biased towards lower values.

Since no sufficient measurements exist to infer the TGSD for any of these eruptions, we consider here a Gaussian distribution ranging from −5–8Φ. We allowed a variability of Md_Φ and σ_Φ on uniform PDF between −1–1Φ and 1–2Φ, respectively. The

NHESSD
2, 2463–2529, 2014

aggregation model was applied, with aggregation coefficients varying between 20–80 % for all bins ≥ 4Φ.

4.1.2 Katla

Numerous eruptions from Katla have been well described and documented, but only a few quantitative constraints exist. Based on Table 2 and Larsen (2010), about 10 historical eruptions produced tephra volumes > 0.1 km^3, with only the 934–940 Eldgjá eruption responsible for a volume > 1 km^3. Since the Eldgjá eruption originated from the surrounding fissure swarm rather than the central volcano, we discard it from the eruption record used in this study, resulting in relevant tephra volumes ranging from 0.1 to 1 km^3. Historical eruptions at Katla are known to have lasted from 2 weeks to 5 months, with most of the tephra produced during the first days. No silicic eruptions were witnessed during historical times, with the last SILK layer erupted 1675 years BP (Larsen et al., 2001).

As a result, a LLERS strategy was applied for Katla volcano in order to assess the hazard related to a future moderate to large basaltic eruption (Table 2). According to the existing literature, plume heights were sampled between 10 and 25 km a.s.l. on a logarithmic PDF (Einarson et al., 1980; Larsen, 2000, 2002; Óladóttir et al., 2008, 2006, 2011; Thordarson and Höskuldsson, 2008). Only the paroxysmal phase was modelled and assumed to last between 1 and 4 days stochastically sampled on a uniform PDF. A volume constraint was set between 0.1 and 1 km^3, converted into a mass constraint between 0.7 and 7×10^{12} kg using a bulk density of 700 $kg\,m^{-3}$. Since no TGSD is available, we used a reconstructed TGSD from the 10 points available for the 1357 eruption in the study of Einarson et al. (1980) using the method of Bonadonna and Houghton (2005), which results in a Md_Φ of −1 and a σ_Φ of 2. However, due to the southward dispersal of the eruption and the narrow area of conservation between the volcano and the sea, these points present a proximal cross-section of the deposit. As a result, a Md_Φ of −1 is considered as a maximum value, and the TGSD adopted here is a Gaussian distribution between −7 and 8Φ with Md_Φ sampled between −1 and 1,

NHESSD
2, 2463–2529, 2014

and σ_Φ sampled between 1 and 2, both on uniform PDF. The resulting distribution is aggregated with an aggregation coefficient sampled between 20 and 80 %. The same TGSD is used for all occurrences of a given run. The time interval between two occurrences was set to 6 h based on the availability of wind data from the Reanalysis databases.

Figure 2 shows the algorithm applied for the LLERS technique and Fig. 5 and Table 3 summarize the ESP for Katla. Figure 5a shows the resulting PDF for plume heights displaying a slight logarithmic trend, and Fig. 5b shows the PDF of eruption duration. Figure 5c displays the PDF for the mass sampling of individual occurrences and results in a strongly logarithmic shape with masses comprised between 10^9 and 6×10^{11} kg. Figure 5d shows the resulting PDF for the mass per run, and Fig. 5e the TGSD at one of the 1000 runs.

4.1.3 Eyjafjallajökull

The limited knowledge of eruptions at Eyjafjallajökull constrains the identification of eruption scenarios. Two prehistoric eruptions are recognized in the field but poorly constrained and three post 17th centuries eruptions were witnessed, amongst which the eruptions of 1612 and 1821–1823 lack any constraint. However, since detailed observations and measurements of eruptive parameters exist for the 2010 eruption, we applied here a LLOES strategy in order to assess the entire range of possible hazard related to the occurrence of a similar eruption.

We model here the 40 days of explosive phase that occurred from 14 April to 20 May 2010. The algorithm used is shown in Fig. 2. The total duration, the time-series of plume heights and the TGSD are deterministically set a priori. Figure 6a shows measurements of plume heights every 6 h for the 40 days of eruption (Arason et al., 2011), converted into MER using the method of Degruyter and Bonadonna (2012) and wind conditions extracted from the NOAA Reanalysis database (Kalnay et al., 1996; Fig. 6b). As a result, the time interval between occurrences within a run was set to 6 h. The TGSD used here is as described by Bonadonna et al. (2011), who reconstructed

NHESSD
2, 2463–2529, 2014

disaggregated and aggregated TGSD by combining ground-based and satellite-based measurements. Here, the same TGSD is used for all runs and does not vary through occurrences.

Following the algorithm in Fig. 2, an eruption date is sampled at each run, after which wind conditions are extracted for the 40 days of the eruption every 6 h. At each occurrence, the MER is calculated accounting for the wind velocity and converted to 6 h-averaged mass. The occurrence is sent to the model, and each run is the sum of the 240 occurrences.

4.1.4 Askja

At least two large tephra deposits associated with strong Plinian eruptions of VEI 5 are recognized at Askja including the 10 ka BP and the 1875 eruptions. Since no accurate mapping or constraints of eruptive parameters are available for the 10 ka BP eruption, we use the 1875 as a reference eruption. Previous studies of Sparks et al. (1981) and Carey et al. (2010) provide an accurate chronology of the different phases of the eruption as well as constraints of the associated eruptive parameters. Two phases are responsible for most of the production of tephra, namely the 1 h-long phreato-Plinian phase Askja C followed 6 h later by the 1.5 h-long Plinian phase Askja D. As a result, we apply here OES strategies modelling two consecutive eruptions separated by a 6 h break.

Figure 2 shows the algorithm developed for a single OES modelling. Here, the hazard related to a 1875-type eruption consists of the sum of one OES for Askja C and one OES for Askja D. All ESP (i.e. plume height, erupted mass, eruption duration and TGSD) are fixed deterministically and are summarized in Table 3 and Fig. 7 for both phases. At each run, an eruption date is sampled and wind data for the consecutive phases are extracted. Both TGSD are aggregated with an aggregation coefficient sampled between 20 and 80 %.

NHESSD
2, 2463–2529, 2014

4.2 Hazard assessment

This section presents the results of the different model runs for all volcanoes. As described in Sect. 3.2, the compilation of probability maps requires a threshold – i.e. either a mass load ($kg\,m^{-2}$), a concentration ($mg\,m^{-3}$), a persistence or an arrival time (h) – in order to calculate the probability of exceeding it for each eruption scenario. Based on the available literature, we use three relevant thresholds for ground accumulation, one for atmospheric concentration, one for persistence and one for arrival time (Table 4). The Supplement contains the entire collection of maps produced including probability maps for atmospheric concentration as well as persistence and arrival times in terms of mean, standard deviation and probability, computed for all FL and for all critical thresholds. In this paper, the resulting impact is not addressed and is left to the companion paper of Scaini et al. (2014).

4.2.1 Ground deposition

Figures 8–11 show the probability maps of exceeding a given threshold of tephra accumulation on the ground for Hekla, Katla, Eyjafjallajökull, and Askja, respectively. In agreement with Fig. 3, there are preferential eastwards dispersals, leaving the Reykjavík area with a negligible probability of being affected by tephra fallout for the volcanoes considered here. As a result, eruptions from volcanoes in the EVZ are likely to affect the area between and east of Gullfoss and Vík í Mýrdal (hereafter referred to as Vík) (Figs. 8–10).

Figure 8 shows the probability maps for Hekla. Figure 8a and b shows the probability of reaching an accumulation of $1\,kg\,m^{-2}$ for the 2000-type and the 1947-type scenarios, respectively. In the case of a 2000-type eruption, there is a $>10\,\%$ probability of reaching such an accumulation up to 50 km east of the volcano and a negligible probability to affect Vík. However, Vík and the southernmost coast have a $\sim 15\,\%$ probability of reaching an equal accumulation for a 1947-type eruption, with the $>10\,\%$ probability line extending 150–200 km eastwards and 50 km westward from the volcano

NHESSD
2, 2463–2529, 2014

(Fig. 8b). This scenario has a ∼ 10 % probability of producing tephra accumulation of 10 kg m^{-3} in the vicinity of Gullfoss (Fig. 8c) and has a 10 % probability of affecting an area with an accumulation of 100 kg m^{-3} 25 km east of the volcano (Fig. 8d).

Figure 9a–c shows the spatial distribution of probabilities of reaching tephra accumulations of 1, 10, and 100 kg m^{-2}, respectively, associated with an eruption at Katla. At Vík, such an eruption results in probabilities of 40 %, ∼ 30 % and 10 % of reaching tephra accumulations of 1, 10, and 100 kg m^{-2}, respectively. The 10 % probability line of reaching a tephra accumulation of 1 kg m^{-2} extends about 200 km northwards in the mainland and eastwards along the coast.

Figure 10 displays the probability distribution for a Eyjafjallajökull 2010-type eruption, resulting in 80 and 20 % probabilities of reaching tephra accumulations of 1 and 10 kg m^{-2} in Vík, respectively (Fig. 10a and b). Due to the low probability level, the map for an accumulation of 100 kg m^{-2} is not shown.

Located in the NVZ, Askja is most likely to impact the eastern part of the country, with half of the territory having a 5–10 % probability of reaching a tephra accumulation of 1 kg m^{-2} should a 1875-type eruption occur (Fig. 11a). The main town under the threat of an eruption of Askja, Egilsstaðir, has ∼ 35 and ∼ 15 % probabilities of reaching tephra accumulations of 1 and 10 kg m^{-2}, respectively (Fig. 11a and b). The towns of Akureyri and Husavik, which both have airports used for internal flights, have 15 and 20 % probabilities of reaching tephra accumulations of 1 kg m^{-2}, respectively. A 1875-type eruption also has a 10 % probability of depositing 100 kg m^{-2} of tephra 50 km east of the vent (Fig. 11c).

Along with probability maps, the hazard related to tephra accumulation can also be expressed as hazard curves, for which the probability of exceeding any tephra accumulation is quantified for a given location. Figure 12 shows hazard curves for relevant eruptions for the locations of Vík, Gullfoss, Akureyri and Egilsstaðir. Although Gullfoss is only a tourist facility, this location was used to assess the probability of tephra accumulation inland. Figure 12a shows that Vík has 15, 40, and 80 % of

NHESSD
2, 2463–2529, 2014

exceeding a tephra accumulation of 1 kg m^{-2} following the considered eruptions of Katla, Hekla 1947-type and Eyjafjallajökull, respectively.

4.2.2 Atmospheric concentration

The hazard assessment for atmospheric concentration is compiled in Figs. 13 and 14, Table 5 and the Supplement. For practical reasons, we present here only probability maps accounting for the presence of ash above a threshold of 2 mg m^{-3} at any FL (Sect. 3, Table 4). Arrival time and persistence are compiled here in the form of probability maps of exceeding arrival and persistence times of 24 and 12 h, respectively. The choice of 24 h for the threshold of arrival time is based on Guffanti et al. (2010), who showed that 89 % of the aircrafts encounters with volcanic ash in the period 1953–2009 occurred within the first 24 h after the onset of the eruption. Since no threshold of persistence time has been outlined since the 2010 crisis of Eyjafjallajökull, we adopted a threshold of 12 h based on qualitative observations found in the literature (e.g. Ulfarsson and Unger, 2011). The Supplement comprises probability maps for other thresholds (i.e. 2×10^{-6} and 0.2 mg m^{-3}) and for separate FL as well as maps of mean and standard deviation of persistence and arrival time. Due to the high computing demand required to run FALL3D in a probabilistic mode for a 40 day long eruption, the Eyjafjallajökull LLOES 2010-type eruption was omitted from the hazard assessment for atmospheric dispersal.

Figure 13a–c shows the results for Hekla. Due to the local dispersal following a 2000-type eruption, only maps for a 1947-type eruption are presented here. Such an eruption would result in a 5–10 % probability of reaching a concentration of 2 mg m^{-3} above the northern Atlantic Ocean and probabilities of reaching London and Oslo of 0.8 and 0.5 % after 13 ± 3 and 17 ± 5 h, respectively (Fig. 13a and b, Table 5). Persistence times for these locations are negligible and are of 3±2 and 5±2 h, respectively (Fig. 13c, Table 5). As shown in the Supplement, similar observations can be made at all separate FLs.

NHESSD
2, 2463–2529, 2014

Following the scenario used here, an eruption at Katla has a 5–20 % probability of affecting the UK and Scandinavia with concentrations of 2 mg m^{-3}. Such concentrations are expected to arrive above London and Oslo after ~ 45 ± 22 h in both cases but persist in the atmosphere for less than 10 h (Fig. 13d–f, Table 5). Due to the long-lasting nature of the Katla scenario, note the high uncertainty on the mean persistence time. The Supplement shows that at separate FL, the impacts of a Katla eruption tend to decrease with altitude.

The atmospheric dispersal of tephra following a 1875-type eruption at Askja is presented in Fig. 13g–i, which results in 5–20 % probabilities to reach a concentration of 2 mg m^{-3} over Scandinavia and Western Europe (UK, Northern France, Netherlands, Belgium, and Western Germany). Such a concentration has a 5–10 % probability of reaching the UK and Scandinavia within 24 h, with mean arrival times above London and Oslo of 22 ± 13 h and 25 ± 12 h, respectively (Fig. 13g and h, Table 5). The airports of Paris and Frankfurt can potentially be impacted after ~ 50 ± 20 h in both cases. In all cases, persistence in the atmosphere would be in the range of ~ 6–8 ± 4 h, with a 5–10 % probability of western Norway to be locally impacted by concentrations of 2 mg m^{-3} persisting for more than 12 h. Similar probability distributions, arrival and persistence times are to be expected at all separate FL (see the Supplement).

4.2.3 Short vs. long-lasting eruptions

In order to compare the potential impact resulting from different types of activity at the selected volcanoes (i.e. short- vs. long-lasting eruptions), this section presents deterministic scenarios based on historical and well-constrained eruptions. Note that these simulations do not aim at presenting "worst-case" scenarios, which would require the combined identification of worst-case eruption scenarios and wind condition, but can be viewed as a comparison of key historical eruptions happening under the same meteorological conditions.

The eruptions of Hekla 1947, Katla 1918, Eyjafjallajökull 2010, and Askja 1875 were selected as case-study scenarios for which sufficient data were available to produce

NHESSD
2, 2463–2529, 2014

a realistic forecast of potential impacts. In order to scale and compare the effect of these eruptions, simulations were run using the wind conditions of Eyjafjallajökull 2010, starting from 14 April and lasting for 10 days. ESP for Eyjafjallajökull and Askja are summarized in Table 3. The 1918 eruption of Katla is the most recent eruption to break through the Mýrdalsjökull ice cap. The available literature suggests that the eruption lasted for 3 weeks, with the most intense tephra production during the first days with plume heights up to 14 km a.s.l. and a total volume varying between 0.7 and 1.6 km^3 (Larsen, 2000; Sturkell et al., 2010). In the absence of any detailed variations of plume heights, radar observations of Arason et al. (2011) were used and scaled to fit observed minimum and maximum plume heights of the Katla 1918 eruption. Using wind conditions specified above and the method of Degruyter and Bonadonna (2012) to estimate the MER, we obtained a total mass of 1.24×10^{12} kg, which is consistent with published volume estimates. Given the similarities between the two systems (Sturkell et al., 2010), the TGSD of Eyjafjallajökull defined by Bonadonna et al. (2011) was also used for this run. ESP for the Hekla 1947 eruption were set using the literature, with a plume height of 27 km a.s.l., a total erupted tephra volume of 0.18 km^3 and a duration of 1.5 h.

Figure 14 summarizes the expected concentrations at FL150 over the main European airports hubs of London Heathrow (EGLL), Paris Charles de Gaulle (LFPG), Amsterdam Schipol (EHAM), Frankfurt (EDDF) Oslo Gardemoen (ENGM), and Copenhagen Kastrup (EKCH) with wind conditions of April 2010, corresponding to the onset of the explosive phase of Eyjafjallajökull 2010 (see Fig. 1 for locations). When interpreting Fig. 14, one should keep in mind that it represents a slice at FL150, namely an altitude of about 4.6 km a.s.l., and the plume height of each scenario should be put in context when interpreting results. Concentration maps for these scenarios for all flights levels can be found in the Supplement.

Figure 14 shows that a Hekla 1947-type eruption bears the largest impact in terms of airborne concentration. A 1947 type eruption would result in concentrations above the threshold of 0.2 $mg\,m^{-3}$ over London, Paris, Amsterdam, Frankfurt, and Copenhagen

NHESSD
2, 2463–2529, 2014

(i.e. 0.35–0.68 mg m^{-3}) arriving after 2–4 days and potentially disrupting the air traffic between 1 and 3 days. Oslo would be the most impacted area with concentration peaks above 10 mg m^{-3}. A Katla 1918-type eruption, characterized by a pulsatory regime with repeated emissions of ash, would potentially be most problematic for the European airspace in terms of duration of disruption. Although most likely reaching concentrations comprising only between 0.1 and 0.25 mg m^{-3}, Fig. 14 reflects the repeated arrival of clouds over time and its potential implications for the management of a volcanic crisis. The eruptions of Askja 1875 and Eyjafjallajökull 2010 only seem to be problematic for Oslo, reaching concentrations above 2 and 0.2 mg m^{-3} respectively.

5 Discussion

5.1 Eruption scenarios and probabilistic strategies

Three steps were taken to develop probabilistic hazard scenarios including (i) the identification of the most probable and potentially problematic eruptive styles at given volcanoes, (ii) the development of adapted algorithms to model each eruption type (Fig. 2), and (iii) the definition of eruption scenarios with constrained ESP (Figs. 4–7). At the selected volcanoes, this led to the identification of both short- and long-lasting eruptions scenarios with both fixed and variable ESP.

5.1.1 Reference time window

For Iceland, the reference period for assessing the eruptive history of volcanic systems was set on historical time for three reasons. Firstly, with a mean eruption of > 20 events per century (Thordarson and Höskuldsson, 2008), the numerous reports and eye-witness accounts since human settlement constitute a valuable source of information when assessing eruptive behaviours and constraining eruption scenarios. Trying to merge such a dataset with an eruption catalogue based on stratigraphic studies

NHESSD
2, 2463–2529, 2014

only results in discrepancies in the completeness of the eruptive record, making any comparison difficult. Secondly, the arid climate of Iceland is prone to fast erosion of freshly fallen deposits, inducing a bias towards large eruptions when trying to assess the pre-historic eruptive activity. Thirdly, since it is recognized that mean eruption frequencies are strongly correlated to glacier load (Albino et al., 2010), any attempt to assess eruptive patterns during older time periods might not be representative of the actual climate and load. As a result, the hazard assessment presented here implies that a future eruption at any of the four volcanoes will follow behaviours similar to the eruptive style displayed in historical times. For instance, considering the possible cycle of evolution of plumbing systems at Katla (Óladóttir et al., 2008), the presented method only attempts to assess the tephra dispersal associated with the current state of the volcano, i.e. a simple plumbing system.

5.1.2 Fixed vs. variable ESP

Amongst chosen volcanoes, a large discrepancy exists in terms of the knowledge of the eruptive history, which is directly related to the frequency of activity during historical times. 17, 10, 3, and 1 eruption of interest (i.e. explosive eruptions at the central vent) occurred during historical times at Hekla, Katla, Eyjafjallajökull and Askja, respectively. On the other hand, a discrepancy also exists in the degree of detail to which eruptions have been mapped and characterized. For example, the single eruption of Askja is thoroughly characterized in terms of chronology of eruptive phases, plume height, erupted volume and TGSD whereas eruptions of Katla are mainly bounded by rough estimates of volume. As a result, the choice of expressing eruptive conditions as either a single set of ESP deterministically defined or as a stochastic sampling on a PDF is made upon the combined knowledge of the eruptive history and the degree of characterization of eruptions.

In the cases of Askja and Eyjafjallajökull, the relatively low frequency of eruptions during historical times did not permit to define ranges of ESP with sufficient degrees of confidence. However, since eruptions of these two volcanoes are thoroughly

NHESSD
2, 2463–2529, 2014

characterized, the hazard assessment performed here using two known and potentially disastrous eruptions can be regarded as "worst-case" in historical time. In the cases of Heka and Katla, the large number of eruptions during historical time provides a good framework for the development of eruption scenarios with varying ESP, but a discrepancy exists in the amount of field studies of eruptions from these two volcanoes. As a result, two eruption scenarios were identified for Hekla based on the historical record to which we were able to assign a mean repose interval, and one eruption scenario was developed for Katla.

5.1.3 Sampling of ESP

Figure 2 shows the algorithms used for producing both short- and long-lasting ERS. Based on the eruptive history, two main constraints are set on the plume height and the erupted mass depending on the eruption scenario (Table 3). In order to avoid the independent sampling of ESP on pre-defined PDF possibly leading to unrealistic eruptive conditions, the erupted mass is indirectly sampled from the MER calculated with the method of Degruyter and Bonadonna (2012) (which depends on both the plume height and wind conditions) and the eruption duration. At each run of the model (Fig. 2), we introduce a test to assess whether the resulting set of ESP fits the initial mass assumptions. Although we constrained the sampling of plume height on a logarithmic distribution as a prior knowledge, the resulting PDF only including values validated by our algorithm shows a wide variety of shapes. For example, Fig. 4a shows that the initial assumptions of erupted mass (i.e. 6.9×10^{9}–6.9×10^{10} kg) for a 2000-type eruption at Hekla for a 0.5–1 h-long eruption cannot be realistic with plume heights under 10 km a.s.l., resulting in (i) a PDF for plume heights biased towards the largest end-members and (ii) a PDF for erupted mass in agreement with an initial assumption of a logarithmic distribution of ESP. Similarly, the 1947-type scenario results in a PDF with a maximum at plume heights of 18–20 km a.s.l. but without solution for plume heights above 27 km a.s.l. satisfying the initial mass (6.9×10^{10}–3.5×10^{11} kg) and duration (0.5–1 h) conditions (Fig. 4d). As a result, this method allows accounting

NHESSD
2, 2463–2529, 2014

for a prior knowledge of the system (i.e. initial choice of a PDF for the sampling of ESP), but helps correcting the sampling of dependent ESPs (i.e. plume height, eruption duration, MER and erupted mass) in order to produce realistic events within an eruption scenario. Here, the combined use of the eruption date, Reanalysis data and the method of Degruyter and Bonadonna (2012) allows calculation of the MER in varying wind conditions and provides a realistic link in the sampling of plume heights and erupted mass.

5.1.4 Short- vs. long-lasting eruption scenarios

Assessing the hazard related to tephra dispersal from long lasting eruption is commonly done using non-steady models but rarely using steady models. Scollo et al. (2013) already used the model TEPHRA2 to evaluate tephra hazard associated with long-lasting violent Strombolian activity at Mt Etna, Italy (e.g. the 21–24 July 2001 eruption). They defined it as weak long-lived plume scenario (OES-WLL and ERS-WLL) with an eruption duration of 4–100 days, in contrast to short-lived plume scenarios (OES-SSL and ERS-SSL) associated with the paroxysmal phase of subplinian eruptions (e.g. the 22 July 1998 eruption).

Here, we developed new algorithms for the sampling of ESP to assess the ground deposition from long-lasting eruptions (Fig. 2). Conceptually, the total ground accumulation calculated with TEPHRA2 consisted of consecutive occurrences of the model run at a given time interval Δt, after which all outputs are summed. With FALL3D, the continuous computation allowed simply updating of the ESP every Δt without interruption. Here, the typical 6 h time resolution of reanalysis datasets conditioned the duration of Δt, implying constant eruption conditions between either different runs or updates.

NHESSD
2, 2463–2529, 2014

5.2 Ground accumulation and atmospheric dispersal

5.2.1 Ground accumulation

Figures 8–11 show the most likely ground deposition patterns for the selected volcanoes for the critical thresholds defined in Table 4. Although no sufficient accumulations to cause structural damage to buildings are predicted (i.e. > 100 kg m^{-2}), deposition of 1–10 kg m^{-2} are likely to occur. Such accumulations are consistent with historical chronicles, which primarily report impact on agricultural activities (e.g. crops destruction, poisoning of animals; Thorarinsson, 1967; Thorarinsson and Sigvaldason, 1972). In addition, eruptions from ice-capped volcanoes such as Katla and Eyjafjallajökull are typically associated with jökullhaups, which are able to cause structural damage to buildings, roads and bridges. If these observations are valid for the selected volcanoes and potentially for most of central vent eruptions with VEI up to 5 – excluding maybe the volcanoes located in the vicinity of Reykjavík and Keflavik, "fires" type eruptions would result in larger magnitude impacts. A review of the environmental changes produced by the Eldgjá fires can be found in Larsen (2000).

Hazard maps produced here also show preferential deposition trends towards the E-ENE, consistent with recent wind observations (Fig. 3). However, compilations of dispersal axes for historical eruptions are available for Hekla (Thorarinsson and Sigvaldason, 1972) and Katla (Larsen, 2000) and show the existence of deposition in all directions around the vents. For example, only 7 out of the 14 historical eruptions of Hekla were dispersed in directions between 0 and 180°, and 8 eruptions dispersed tephra in a 340–20° sector. Similarly, half of the historical eruptions of Katla were dispersed and deposited with a bearing comprised between 0 and 180°. By comparing our probability maps for Eyjafjallajökull to the isomass maps of Gudmundsson et al. (2012) compiled for land deposition in the period 14 April–22 May, we observe a ground deposition slightly more directed towards the south than predicted by our model (Fig. 10). However, deposition observed on the ground for both 1 and 10 kg m^{-2}

NHESSD
2, 2463–2529, 2014

(converted from the isopach maps of Gudmundsson et al., 2012 with a density of 1400 kg m^{-3}) fall between our 10 and 30 % probability lines. Similarly, the isopach maps and ground measurements for the C and D units of the Askja 1875 produced by Carey et al. (2010) are in agreement with our 10 and 20 % probability lines for ground tephra accumulations of 1 and 10 kg m^{-2} (Fig. 11).

5.2.2 Atmospheric concentration

Figure 13 summarizes the most likely dispersal trends, here again in agreement with the wind transect of Fig. 2, and shows that the areas most probably affected by far-range dispersal of ash are Scandinavia and the northern UK. Such results are in agreement with the compilation of the tephrochronological studies of Swindles et al. (2011), who show that the past 7000 years of volcanic activity in Iceland resulted in the identification of 38, 33, and 11 tephra layers in Scandinavia, Ireland and Great Britain, respectively. As suggested by Lacasse (2001), Scandinavia is subject to zonal airflow, whereas Ireland is more likely to be affected than the rest of Europe as it is most probably in the path of anticyclonic airflows from Iceland. As a result, minimum estimates provided by Swindles et al. (2011) show that, based on the record of the past 1000 years, northern Europe is affected by volcanic ash with a mean return interval of 56 ± 9 years and that there is a 16 % probability of tephra fallout every decade based on a Poisson model.

When using a deterministic approach, Fig. 14 shows that amongst the selected eruptions, an eruption of Hekla 1947 is the most likely to produce critical concentrations above the main European airports. Interestingly, scaling Hekla 1947 with the two main phases of Askja 1875 reveals that an erupted volume falling within the boundaries of a low VEI 4 (Hekla 1947) can produce concentrations more than one order of magnitude larger than an eruption of low-medium VEI 5 (Askja 1875). For example, London Heathrow would suffer ash concentrations of 0.68 and 0.025 mg m^{-3} following eruptions of Hekla 1947 and Askja 1875, respectively (Fig. 14). Similarly, Davies et al. (2010) report that five eruptions of Hekla with volumes varying between 0.18 and

NHESSD
2, 2463–2529, 2014

0.33 km^3 produced tephra beds in Norway, Scotland and Finland, more than 1500 km beyond the source. Such observations support the growing idea that the tephra volume of an eruption is not the primary factor controlling the distal dispersal of fine ash and that the TGSD, the nature of the fragmentation process (i.e. dry vs. phreatomagmatic) and the weather patterns play important roles (Davies et al., 2010; Swindles et al., 2011).

The concept of defining critical thresholds, typically 0, 0.2 or 2 mg m^{-3} depending on the approach adopted, implies that the hazard level is at its maximum once the concentration thresholds has been reached. If, for instance, a value of 0.2 mg m^{-3} is adopted as critical, the shape of the curve above the threshold for the eruption of Hekla 1947 displayed on Fig. 14 does not provide any relevant information as the level of maximum impact is reached. However, for crisis management purposes, the duration during which concentrations are above the threshold becomes critical. In this perspective, the eruption type has a major control on the hazard and the potential associated consequences. For example, concentration plots using a deterministic approach for all flight levels shown in the Supplement illustrate how short-lasting and intense Plinian eruptions result in single peaks of critical concentration typically lasting for a couple of days, reaching up to 12 mg m^{-3} above the Oslo airport following a Hekla 1947 eruption. In contrast, an eruption of Katla 1918, although not reaching such high levels of critical thresholds, results in more diffuse signals spanning over longer periods of time over single geographic points. When considering a 3-D volume above the European territory representing the airspace and observing the potential disruptions from a management perspective, continuous emission of tephra with a pulsatory regime, though not producing the high concentrations of Plinian eruptions, are potentially able to become more problematic than short-lasting powerful eruptions.

NHESSD
2, 2463–2529, 2014

6 Conclusions

The present work highlights the challenges of achieving a multi-scale hazard assessment from multiple and heterogeneous sources in order to compare and combine outcomes of the most likely range of possible eruptions. For the selected volcanoes, we were able to define both semi-probabilistic (i.e. stochastic sampling of wind conditions and ESP deterministically fixed) and fully-probabilistic (i.e. stochastic sampling of both wind profiles and ESP) eruption scenarios based on the available data. In each case, we developed new algorithms to assist the identification of eruption parameters for both short- and long-lasting eruptions, which help achieve the sampling of realistic ESP and account for particle aggregation processes. For the atmospheric dispersal of fine ash, a sound deterministic approach demonstrated the different hazards posed by short- and long-lasting eruptions and showed the importance of the potential disruption time over high concentrations. As a result, the outcomes of this work constitute a first step towards an improved management of future volcanic crises, accounting for most critical aspects of both the geological and atmospheric science sides of the problem. The second step toward a sound impact and risk assessment typically involves the identification of the exposed elements and their vulnerability to the stress constituted by ground tephra accumulation and distal atmospheric ash. Such an approach is tackled in a companion paper by Scaini et al. (2014).

In terms of hazard assessment, we can conclude that:

- Eruption scenarios and ESP must be defined using probabilistic strategies based on strong field evidence.
- The erupted tephra volume is not the primary control on the dispersal.
- Based on probabilistic scenarios (e.g. OES, ERS), Askja represents the most hazardous volcano.

NHESSD
2, 2463–2529, 2014

– Based on deterministic scenarios, Hekla is likely to produce the larger atmospheric concentrations of ash but Katla will result in longer disruptions of air traffic.

– At the Icelandic scale, expected accumulations will mainly be a concern for electrical power-lines and agricultural activities (i.e. accumulations of 10 $kg\,m^{-2}$).

Supplementary material related to this article is available online at http://www.nat-hazards-earth-syst-sci-discuss.net/2/2463/2014/nhessd-2-2463-2014-supplement.pdf.

Acknowledgements. We kindly acknowledge Guðrún Larsen and Þorvaldur Þórðarson for sharing their immense knowledge of the stratigraphy and Bergrún Óladóttir, Jónas Guðnason and Johanne Schmith for their help in reviewing and translating the literature. S. Biass is supported by SNF (#200021-129997) and ESF/MemoVolc (#5193) subsides. C. Scaini is partly supported by the Spanish Research Project ATMOST (CGL2009-10244) and by the SNF (IZK0Z2_ 142343). Simulations have been done at the Earth Sciences Department of Geneva University and the Barcelona Supercomputing Center (BSC-CNS) using the MareNostrum supercomputer.

References

Albino, F., Pinel, V., and Sigmundsson, F.: Influence of surface load variations on eruption likelihood: application to two Icelandic subglacial volcanoes, Grímsvötn and Katla, Geophys. J. Int., 181, 1510–1524, doi:10.1111/j.1365-246X.2010.04603.x, 2010.

Allen, R. M., Nolet, G., Morgan, W. J., Vogfjörd, K., Bergsson, B. H., Erlendsson, P., Foulger, G. R., Jakobsdóttir, S., Julian, B. R., Pritchard, M., Ragnarsson, S., and Stefansson, R.: The thin hot plume beneath Iceland, Geophys. J. Int., 137, 51–63, 1999.

Arason, P., Petersen, G. N., and Bjornsson, H.: Observations of the altitude of the volcanic plume during the eruption of Eyjafjallajökull, April–May 2010, Earth Syst. Sci. Data, 3, 9–17, doi:10.5194/essd-3-9-2011, 2011.

NHESSD

2, 2463–2529, 2014

Bagheri, G. H., Bonadonna, C., Manzella, I., Pontelandolfo, P., and Haas, P.: Dedicated vertical wind tunnel for the study of sedimentation of non-spherical particles, Rev. Sci. Instrum., 84, 054501–054501–12, 2013.

Bebbington, M., Cronin, S. J., Chapman, I., and Turner, M. B.: Quantifying volcanic ash fall hazard to electricity infrastructure, J. Volcanol. Geotherm. Res., 177, 1055–1062, doi:10.1016/j.jvolgeores.2008.07.023, 2008.

Biass, S. and Bonadonna, C.: A quantitative uncertainty assessment of eruptive parameters derived from tephra deposits: the example of two large eruptions of Cotopaxi volcano, Ecuador, B. Volcanol., 73, 73–90, doi:10.1007/s00445-010-0404-5, 2011.

Biass, S. and Bonadonna, C.: A fast GIS-based risk assessment for tephra fallout: the example of Cotopaxi volcano, Ecuador-Part I: probabilistic hazard assessment, Nat. Hazards, 65, 477–495, doi:10.1007/s11069-012-0378-z, 2013.

Biass, S., Frischknecht, C., and Bonadonna, C.: A fast GIS-based risk assessment for tephra fallout: the example of Cotopaxi volcano, Ecuador – Part II: vulnerability and risk assessment, Nat. Hazards, 65, 497–521, doi:10.1007/s11069-012-0457-1, 2013.

Björnsson, H., Pálsson, F., and Guðmundsson, M. T.: Surface and bedrock topography of the Mýrdalsjökull ice cap, Jökull, 49, 29–46, 2000

Blong, R. J.: Volcanic Hazards, a Sourcebook on the Effects of Eruptions, Academic Press, Orlando. 1984.

Bonadonna, C.: Probabilistic modelling of tephra dispersion, Special Publications of IAVCEI, 1. Geological Society, London, 2006.

Bonadonna, C. and Houghton, B. F.: Total grain-size distribution and volume of tephra-fall deposits, B. Volcanol., 67, 441–456, doi:10.1007/s00445-004-0386-2, 2005.

Bonadonna, C. and Phillips, J. C.: Sedimentation from strong volcanic plumes, J. Geophys. Res., 108, 2340, doi:10.1029/2002JB002034, 2003.

Bonadonna, C., Connor, C. B., Houghton, B. F., Connor, L., Byrne, M., Laing, A., and Hincks, T. K.: Probabilistic modeling of tephra dispersal: Hazard assessment of a multiphase rhyolitic eruption at Tarawera, New Zealand, J. Geophys. Res., 110, B03203, doi:10.1029/2003JB002896, 2005.

Bonadonna, C., Folch, A., Loughlin, S., and Puempel, H.: Future developments in modelling and monitoring of volcanic ash clouds: outcomes from the first IAVCEI-WMO workshop on Ash Dispersal Forecast and Civil Aviation, B. Volcanol., 74, 1–10, doi:10.1007/s00445-011-0508-6, 2012.

NHESSD

2, 2463–2529, 2014

Bonadonna, C., Genco, R., Gouhier, M., Pistolesi, M., Cioni, R., Alfano, F., Hoskuldsson, A., and Ripepe, M.: Tephra sedimentation during the 2010 Eyjafjallajökull eruption (Iceland) from deposit, radar, and satellite observations, J. Geophys. Res., 116, B12202, doi:10.1029/2011JB008462, 2011.

Bonadonna, C., Macedonio, G., and Sparks, R. S. J.: Numerical modelling of tephra fallout associated with dome collapses and Vulcanian explosions: application to hazard assessment on Montserrat, in: The eruption of Soufrière Hills Volcano, Montserrat, from 1995 to 1999, vol. 21, edited by: Druitt, T. and Kokelaar, B., Geological Society, London, Memoirs, London, 483–516, 2002.

Bonasia, R., Capra, L., Costa, A., Macedonio, G., and Saucedo, R.: Tephra fallout hazard assessment for a Plinian eruption scenario at Volcan de Colima (Mexico), J. Volcanol. Geotherm. Res., 203, 12–22, doi:10.1016/j.jvolgeores.2011.03.006, 2011.

Brown, R. J., Bonadonna, C., and Durant, A. J.: A review of volcanic ash aggregation, Phys. Chem. Earth, 45–46, 65–78, doi:10.1016/j.pce.2011.11.001, 2012.

Budd, L., Griggs, S., Howarth, D., and Ison, S.: A Fiasco of Volcanic Proportions? Eyjafjallajökull and the Closure of European Airspace, Mobilities, 6, 31–40, doi:10.1080/17450101.2011.532650, 2013.

Capra, L., Norini, G., Groppelli, G., Macias, J., and Arce, J.: Volcanic hazard zonation of the Nevado de Toluca volcano, Mexico, J. Volcanol. Geoth. Res., 176, 469–484, doi:10.1016/j.jvolgeores.2008.04.016, 2008.

Carey, R. J., Houghton, B. F., and Thordarson, T.: Contrasting styles of welding observed in the proximal Askja 1875 eruption deposits I: Regional welding, J. Volcanol. Geoth. Res., 171, 1–19, doi:10.1016/j.jvolgeores.2007.11.020, 2008.

Carey, R., Houghton, B., and Thordarson, T.: Tephra dispersal and eruption dynamics of wet and dry phases of the 1875 eruption of Askja Volcano, Iceland, B. Volcanol., 72, 259–278, 2010.

Carey, S. N. and Sigurdsson, H.: Influence of particle aggregation on deposition of distal tephra from the MAy 18, 1980, eruption of Mount St. Helens volcano, J. Geophys. Res., 87, 7061–7072, doi:10.1029/JB087iB08p07061, 1982.

Cioni, R., Longo, A., Macedonio, G., Santacroce, R., Sbrana, A., Sulpizio, R., and Andronico, D.: Assessing pyroclastic fall hazard through field data and numerical simulations: example from Vesuvius, J. Geophys. Res., 108, 2063, doi:10.1029/2001JB000642, 2003.

NHESSD
2, 2463–2529, 2014

Connor, C., Hill, B., and Winfrey, B.: Estimation of volcanic hazards from tephra fallout, Nat. Hazards, 2, 33–42, 2001.

Connor, L. J. and Connor, C. B.: Inversion is the key to dispersion: understanding eruption dynamics by inverting tephra fallout, in: Statistics in Volcanology, Special Publications of IAVCEI, edited by: Mader, H. M., Connor, C. B., Coles, S. G., Connor, L. J., 1. Geological Society, London, 231–242, 2006.

Cornell, W., Carey, S., and Sigurdsson, H.: Computer simulation of transport and deposition of the campanian Y-5 ash, J. Volcanol. Geoth. Res., 17, 89–109, 1983.

Costa, A., Macedonio, G., and Folch, A.: A three-dimensional Eulerian model for transport and deposition of volcanic ashes, Earth Planet. Sc. Lett., 241, 634–647, doi:10.1016/j.epsl.2005.11.019, 2006.

Costa, A., Dell'Erba, F., Di Vito, M., Isaia, R., Macedonio, Orsi, G., and Pfeiffer, T.: Tephra fallout hazard assessment at the Campi Flegrei caldera (Italy), B. Volcanol., 71, 259–273, 2009.

Costa, A., Folch, A., and Macedonio, G.: A model for wet aggregation of ash particles in volcanic plumes and clouds: 1. Theoretical formulation, J. Geophys. Res., 115, B09201, doi:10.1029/2009JB007175, 2010.

Costa, A., Folch, A., Macedonio, G., Giaccio, B., Isaia, R., and Smith, V. C.: Quantifying volcanic ash dispersal and impact from Campanian Ignimbrite super-eruption, Geophys. Res. Lett., 39, L10310, doi:10.1029/2012GL051605, 2012.

Davies, S. M., Larsen, G., Wastegard, S., Turney, C. S., Hall, V. A., Coyle, L., and Thordarson, T.: Widespread dispersal of Icelandic tephra: how does the Eyjafjoll eruption of 2010 compare to past Icelandic events?, J. Quaternary Sci., 25, 605–611, 2010.

Degruyter, W. and Bonadonna, C.: Improving on mass flow rate estimates of volcanic eruptions, Geophys Res Lett, 39, L16308, doi:10.1029/2012GL052566, 2012.

Dugmore, A. J., Newton, A. J., Smith, K. T., and Mairs, K.-A.: Tephrochronology and the late Holocene volcanic and flood history of Eyjafjallajökull, Iceland, J. Quaternary Sci., 28, 237–247, doi:10.1002/jqs.2608, 2013.

Einarson, E., Larsen, G., and Thorarinsson, S.: The Solheimar tephra layer and the Katla eruption of 1357, Acta Naturalia Islandica, 2, 2–24, 1980.

Eliasson, J., Larsen, G., Tumi Gudmundsson, M., and Sigmundsson, F.: Probabilistic model for eruptions and associated flood events in the Katla caldera, Iceland, Computat. Geosci., 10, 179–200, doi:10.1007/s10596-005-9018-y, 2006.

NHESSD

2, 2463–2529, 2014

Ewert, J. W.: System for ranking relative threats of US volcanoes, Nat. Hazards Rev., 8, 112–124, doi:10.1061/(ASCE)1527-6988(2007)8:4(112), 2007.
Folch, A.: A review of tephra transport and dispersal models: evolution, current status, and future perspectives, J. Volcanol. Geoth. Res., 235–236, 96–115, 2012.
Folch, A. and Sulpizio, R.: Evaluating long-range volcanic ash hazard using supercomputing facilities: application to Somma-Vesuvius (Italy), and consequences for civil aviation over the Central Mediterranean Area, B. Volcanol., 72, 1039–1059, doi:10.1007/s00445-010-0386-3, 2010.
Folch, A., Costa, A., and Macedonio, G.: FALL3D: a computational model for transport and deposition of volcanic ash, Comput. Geosci., 35, 1334–1342, doi:10.1016/j.cageo.2008.08.008, 2009.
Folch, A., Costa, A., Durant, A., and Macedonio, G.: A model for wet aggregation of ash particles in volcanic plumes and clouds: 2. Model application, J. Geophys. Res., 115, B09202, doi:10.1029/2009JB007176, 2010.
Ganser, G. H.: A rational approach to drag prediction of spherical and nonspherical particles, Powder Technol., 77, 143–152, 1993.
Gronvold, K., Larsen, G., Einarsson, P., Thorarinsson, S., and Saemundsson, K.: The Hekla eruption 1980–1981, B. Volcanol., 46, 349–363, doi:10.1007/BF02597770, 1983.
Gudmundsson, A.: Infrastructure and mechanics of volcanic systems in Iceland, J. Volcanol. Geoth. Res., 64, 1–22, 1995a.
Gudmundsson, A.: Ocean-ridge discontinuities in Iceland, J. Geol. Soc. London, 152, 1011–1015, 1995b.
Gudmundsson, A.: Dynamics of Volcanic Systems in Iceland: example of Tectonism and Volcanism at Juxtaposed Hot Spot and Mid-Ocean Ridge Systems, Annu. Rev. Earth Planet. Sci., 28, 107–140, doi:10.1146/annurev.earth.28.1.107, 2000.
Gudmundsson, A., Óskarsson, N., Gronvold, K., Saemundsson, K., Sigurdsson, O., Stefansson, R., Gislason, S., Einarsson, P., Brandsdottir, B., Larsen, G., Johannesson, H., and Thordarson, T.: The 1991 eruption of Hekla, Iceland, B. Volcanol., 54, 238–246, doi:10.1007/BF00278391, 1992.
Gudmundsson, M. T., Pedersen, R., Vogfjörd, K., Thorbjarnardóttir, B., Jakobsdóttir, S., and Roberts, M. J.: Eruptions of Eyjafjallajökull Volcano, Iceland, Eos T. Am. Geophys. Un., 91, 190–191, doi:10.1029/2010EO210002, 2010.

NHESSD
2, 2463–2529, 2014

Gudmundsson, M. T., Thordarson, T., Höskuldsson, Á., Larsen, G., Björnsson, H., Prata, F. J., Oddsson, B., Magnússon, E., Högnadóttir, T., Petersen, G. N., Hayward, C. L., Stevenson, J. A., and Jónsdóttir, I.: Ash generation and distribution from the April–May 2010 eruption of Eyjafjallajökull, Iceland, Sci. Rep., 2, doi:10.1038/srep00572, 2012.

Guffanti, M., Casadevall, T. J., Budding, K.: Encounters of aircraft with volcanic ash clouds: a compilation of known incidents, 1953–2009, US Geological Survey Data Series 545, available at: http://pubs.usgs.gov/ds/545/, last access: 19 March 2014, 2010.

Hall, M. and von Hillebrandt, C.: Mapa de los peligros volcanicos potenciales asociados con el volcan Cotopaxi: zona norte and zona sur, Instituto Geofisico, Quito, 1988.

Hartley, M. E. and Thordarson, T.: Formation of Öskjuvatn caldera at Askja, North Iceland: mechanism of caldera collapse and implications for the lateral flow hypothesis, J. Volcanol. Geoth. Res., 227–228, 85–101, 2012.

Hildreth, W. and Drake, R.: Volcán Quizapu, Chilean Andes, B. Volcanol., 54, 93–125, 1992.

Hjartardóttir, Á., Einarsson, P., and Sigurdsson, H.: The fissure swarm of the Askja volcanic system along the divergent plate boundary of N Iceland, B. Volcanol., 71, 961–975, doi:10.1007/s00445-009-0282-x, 2009.

Höskuldsson, Á., Óskarsson, N., Pedersen, R., Grönvold, K., Vogfjörð, K., and Ólafsdóttir, R.: The millennium eruption of Hekla in February 2000, B. Volcanol., 70, 169–182, 2007.

Hurst, T. and Smith, W.: A Monte Carlo methodology for modelling ashfall hazards, J. Volcanol. Geoth. Res., 138, 393–403, doi:10.1016/j.jvolgeores.2004.08.001, 2004.

IVATF: First meeting of the International Volcanic Ash Task Force (IVATF), IVATF/1-REPORT, http://www.icao.int/safety/meteorology/ivatf/Meeting%20MetaData/Final.Alltext.pdf, last access: 19 February 2014, 2010.

Jenkins, S., Magill, C., McAneney, J., and Blong, R.: Regional ash fall hazard I: a probabilistic assessment methodology, B. Volcanol., 74, 1699–1712, doi:10.1007/s00445-012-0627-8, 2012a.

Jenkins, S., McAneney, J., Magill, C., and Blong, R.: Regional ash fall hazard II: Asia-Pacific modelling results and implications, B. Volcanol., 74, 1713–1727, doi:10.1007/s00445-012-0628-7, 2012b.

Kalnay, E., Kanamitsu, M., Kistler, R., and Collins, W.: The NCEP/NCAR 40-year reanalysis project, B. Am. Meteorol. Soc., 77, 437–471, 1996.

Lacasse, C.: Influence of climate variability on the atmospheric transport of Icelandic tephra in the subpolar North Atlantic, Global Planet. Change, 29, 31–55, 2001.

NHESSD
2, 2463–2529, 2014

Larsen, G.: Holocene eruptions within the Katla volcanic system, south Iceland: characteristics and environmental impact, Jökull, 49, 1–28, 2000.
Larsen, G.: A brief overview of eruptions from ice-covered and ice-capped volcanic systems in Iceland during the past 11 centuries: frequency, periodicity and implications, Geological Society, London, Special Publications, 202, 81–90, 2002.
Larsen, G.: Katla – tephrochronology and eruption history, in: The Mýrdalsjökull ice cap, Iceland: glacial processes, sediments and landforms on an active volcano, Development in Quaternary Science, edited by: Schomacker, A., Krüger, J., and Kjær, K., 13, Elsevier, Amsterdam, 23–49, 2010.
Larsen, G. and Eirìksson, J.: Late Quaternary terrestrial tephrochronology of Iceland – frequency of explosive eruptions, type and volume of tephra deposits, J. Quaternary Sci., 23, 109–120, doi:10.1002/jqs.1129, 2008.
Larsen, G., Newton, A. J., Dugmore, A. J., and Vilmundardottir, E. G.: Geochemistry, dispersal, volumes and chronology of Holocene from the Katla volcanic silicic tephra layers system, Iceland, J. Quaternary Sci., 16, 119–132, 2001.
Lirer, L., Petrosino, P., and Alberico, I.: Hazard and risk assessment in a complex multi-source volcanic area: the example of the Campania Region, Italy, B. Volcanol., 72, 411–429, doi:10.1007/s00445-009-0334-2, 2010.
Loughlin, S. C.: Facies analysis of proximal subglacial and proglacial volcaniclastic successions at the Eyjafjallajökull central volcano, southern Iceland, Geological Society, London, Special Publications, 202, 149–178, 2002.
Macedonio, G., Costa, A., and Folch, A.: Ash fallout scenarios at Vesuvius: numerical simulations and implications for hazard assessment, J. Volcanol. Geoth. Res., 178, 366–377, doi:10.1016/j.jvolgeores.2008.08.014, 2008.
Mattsson, H. and Höskuldsson, Á.: Geology of the Heimaey volcanic centre, south Iceland: early evolution of a central volcano in a propagating rift?, J. Volcanol. Geoth. Res., 127, 55–71, 2003.
Marti, J., Spence, R., Calogero, E., Ordoñez, A., Felpeto, A., and Baxter, P.: Estimating building exposure and impact to volcanic hazards in Icod de los Vinos, Tenerife (Canary Islands), J. Volcanol. Geoth. Res., 178, 553–561, doi:10.1016/j.jvolgeores.2008.07.010, 2008.
Marzocchi, W., Sandri, L., Gasparini, P., Newhall, C., and Boschi , E.: Quantifying probabilities of volcanic events: the example of volcanic hazard at Mount Vesuvius, J. Geophys. Res, 109, B11201, doi:10.1029/2004JB003155, 2004.

NHESSD
2, 2463–2529, 2014

Óladóttir, B. A., Larsen, G., Þórðarson, Þ., and Sigmarsson, O.: The Katla volcano S-Iceland: holocene tephra stratigraphy and eruption frequency, Jökull, 55, 53–74, 2006.
Óladóttir, B. A., Sigmarsson, O., Larsen, G., and Thordarson, T.: Katla volcano, Iceland: magma composition, dynamics and eruption frequency as recorded by Holocene tephra layers, B. Volcanol., 70, 475–493, 2008.
Óladóttir, B., Larsen, G., and Sigmarsson, O.: Holocene volcanic activity at Grímsvötn, Bárdarbunga and Kverkfjöll subglacial centres beneath Vatnajökull, Iceland, B. Volcanol., 73, 1187–1208, doi:10.1007/s00445-011-0461-4, 2011.
Rao, C. R. and Krishnaiah, P. R. (Eds.): Handbook of Statistics 6, Sampling (Vol. 6), Elsevier, Amsterdam, 1994.
Rose, W. I. and Durant, A. J.: Fate of volcanic ash: aggregation and fallout, Geology, 39, 895–896, 2011.
Scaini, C., Folch, A., and Navarro, M.: Tephra hazard assessment at Concepción Volcano, Nicaragua, J. Volcanol. Geoth. Res., 219–220, 41–51, doi:10.1016/j.jvolgeores.2012.01.007, 2012.
Scaini, C., Biass, S., Galderisi, A., Bonadonna, C., Folch, A., Smith, K., and Hoskuldsson, A.: A multi-scale risk assessment for tephra fallout and airborne concentration from multiple Icelandic volcanoes – Part 2: Vulnerability and impact, Nat. Hazards Earth Syst. Sci. Discuss., 2, 2531–2595, doi:10.5194/nhessd-2-2531-2014, 2014.
Scollo, S., Coltelli, M., Bonadonna, C., and Del Carlo, P.: Tephra hazard assessment at Mt. Etna (Italy), Nat. Hazards Earth Syst. Sci., 13, 3221–3233, doi:10.5194/nhess-13-3221-2013, 2013.
Scollo, S., Tarantola, S., Bonadonna, C., Coltelli, M., and Saltelli, A.: Sensitivity analysis and uncertainty estimation for tephra dispersal models, J. Geophys. Res., 113, B06202, doi:10.1029/2006JB004864, 2008.
Sigmundsson, F., Hreinsdóttir, S., Hooper, A., Árnadóttir, T., Pedersen, R., Roberts, M. J., Óskarsson, N., Auriac, A., Decriem, J., Einarsson, P., Geirsson, H., Hensch, M., Ófeigsson, B. G., Sturkell, E., Sveinbjörnsson, H., and Feigl, K. L.: Intrusion triggering of the 2010 Eyjafjallajökull explosive eruption, Nature, 468, 426–430, doi:10.1038/nature09558, 2010.
Sigvaldason, G.: Volcanic and tectonic processes coinciding with glaciation and crustal rebound: an early Holocene rhyolitic eruption in the Dyngjufjöll volcanic centre and the

NHESSD
2, 2463–2529, 2014

formation of the Askja caldera, north Iceland, B. Volcanol., 64, 192–205, doi:10.1007/s00445-002-0204-7, 2002.
Simkin, T. and Siebert, L.: Volcanoes of the World, Geoscience Press, Tucson, AZ, 1994.
Soosalu, H., Jónsdóttir, K., and Einarsson, P.: Seismicity crisis at the Katla volcano, Iceland – signs of a cryptodome?, J. Volcanol. Geoth. Res., 153, 177–186, 2006.
Sparks, R., Wilson, L., and Sigurdsson, H.: The pyroclastic deposits of the 1875 eruption of Askja, Iceland, Philos. T. Roy. Soc. Lond., 299, 241–273, 1981.
Spence, R. J. S., Kelman, I., Baxter, P. J., Zuccaro, G., and Petrazzuoli, S.: Residential building and occupant vulnerability to tephra fall, Nat. Hazards Earth Syst. Sci., 5, 477–494, doi:10.5194/nhess-5-477-2005, 2005.
Sturkell, E., Einarsson, P., Roberts, M. J., Geirsson, H., Gudmundsson, M. T., Sigmundsson, F., Pinel, V., Guðmundsson, G. B., Ólafsson, H., and Stefansson, R.: Seismic and geodetic insights into magma accumulation at Katla subglacial volcano, Iceland: 1999 to 2005, J. Geophys. Res., 113, B03212, doi:10.1029/2006JB004851, 2008.
Sturkell, E., Einarsson, P., Sigmundsson, F., Hooper, A., Ófeigsson, B. G., Geirsson, H., and Ólafsson, H.: Katla and Eyjafjallajökull volcanoes, in: Developments in Quaternary Sciences, vol. 13, edited by: Schomacker, A., Krüger, J., and Kjær, H., Elsevier, 5–21, 2010.
Sulpizio, R., Folch, A., Costa, A., Scaini, C., and Dellino, P.: Hazard assessment of far-range volcanic ash dispersal from a violent Strombolian eruption at Somma-Vesuvius volcano, Naples, Italy: implications on civil aviation, B. Volcanol., 74, 2205–2218, doi:10.1007/s00445-012-0656-3, 2012.
Suzuki, T.: A theoretical model for dispersion of tephra, in: Arc Volcanism: Physics and Tectonics, edited by: Shimozuru, D., and Yokoyama S. D., Terra Sci. Publ. Comp. (TERRAPUB), Tokyo, 95–113, 1983.
Swindles, G. T., Lawson, I. T., Savov, I. P., Connor, C. B., and Plunkett, G.: A 7000 yr perspective on volcanic ash clouds affecting northern Europe, Geology, 39, 887–890, doi:10.1130/G32146.1, 2011.
Taddeucci, J., Scarlato, P., Montanaro, C., Cimarelli, C., Del Bello, E., Freda, C., Andronico, D., Gudmundsson, M. T., and Dingwell, D. B.: Aggregation-dominated ash settling from the Eyjafjallajokull volcanic cloud illuminated by field and laboratory high-speed imaging, Geology, 39, 891–894, doi:10.1130/G32016.1, 2011.
Thorarinsson, S.: The eruption of Hekla 1947–1948, Vinsindafélag Islendinga, 1–199, 1967.

NHESSD
2, 2463–2529, 2014

Thorarinsson, S. and Sigvaldason, G. E.: The Hekla Eruption of 1970, B. Volcanol., 36, 269–288, doi:10.1007/BF02596870, 1972.
Thordarson, T. and Höskuldsson, Á.: Postglacial volcanism in Iceland, Jökull, 58, 197–228, 2008.
Thordarson, T. and Larsen, G.: Volcanism in Iceland in historical time: volcano types, eruption styles and eruptive history, J. Geodyn., 43, 118–152, 2007.
Ulfarsson, G. and Unger, E.: Impacts and responses of Icelandic aviation to the 2010 Eyjafjallajökull volcanic eruption, J. Trans. Res. Board., 2214–1:144–151, doi:10.3141/2214-18, 2011.
Van Eaton, A. R. and Wilson, C. J. N.: The nature, origins and distribution of ash aggregates in a large-scale wet eruption deposit: Oruanui, New Zealand, J. Volcanol. Geoth. Res., 250, 129–154, doi:10.1016/j.jvolgeores.2012.10.016, 2013.
Van Eaton, A. R., Muirhead, J. D., Wilson, C. J. N., and Cimarelli, C.: Growth of volcanic ash aggregates in the presence of liquid water and ice: an experimental approach, B. Volcanol., 74, 1963–1984, doi:10.1007/s00445-012-0634-9, 2012.
Vésteinsson, O.: The archaeology of Landnám icelandic early settlement, in: Vikings: The North Atlantic Saga, edited by: Fitzhugh, W. W. and Ward, E., Smithsonian Institution Press, Washington DC, 164–174, 2000.
Vink, G. E.: A hotspot model for Iceland and the Vøring Plateau, J. Geophys. Res., 89, 9949–9959, doi:10.1029/JB089iB12p09949, 1984.
Volentik, A., Connor, C. B., Connor, L. J., and Bonadonna, C.: Aspects of volcanic hazard assessment for the Bataan nuclear power plant, Luzon peninsula, Philippines, in: Volcanic and Tectonic Hazard Assessment for Nuclear Facilities, Connor, C. B., Chapman, N., and Connor, L. J., Cambridge University Press, Cambridge, 229–256, 2009.
White, R. S., Bown, J. W., and Smallwood, J. R.: The temperature of the Iceland plume and origin of outward-propagating V-shaped ridges, J. Geol. Soc. London, 152, 1039–1045, 1995.
Wilkinson, S., Dunn, S., and Ma, S.: The vulnerability of the European air traffic network to spatial hazards, Nat. Hazards, 60, 1027–1036, 2012.
Wilson, T., Stewart, C., and Sword-Daniels, V.: Volcanic ash impacts on critical infrastructure, Phys. Chem. Earth, 45–46, 5–23, doi:10.1016/j.pce.2011.06.006, 2011.
Wolfe, C. J., Bjarnason, I. Th., VanDecar, J. C., and Solomon, S. C.: Seismic structure of the Iceland mantle plume, Nature, 385, 245–247, doi:10.1038/385245a0, 1997.

NHESSD
2, 2463–2529, 2014

Yu, H., Xu, J., Luan, P., Zhao, B., and Pan, B.: Probabilistic assessment of tephra fallout hazard at Changbaishan volcano, Northeast China, Nat. Hazards, 1–20, doi:10.1007/s11069-013-0683-1, 2013.

NHESSD
2, 2463–2529, 2014

Table 1. Historical eruptions at the central volcano of Hekla (Thordarson and Larsen, 2007) and references therein. Tephra volumes are recorded as "freshly fallen" (i.e. 40 % larger than volumes of old eruptions inferred from field mapping; Thorarinsson, 1967). Following the typical pattern of mixed eruptions at Hekla, plume heights correspond to the maximum altitude reached a few minutes after the onset of the eruption. NA: Not available.

Eruption year	Tephra (km^3)	Max plume height (km a.s.l.)	Preceding interval (years)
2000	0.01	12	9
1991	0.02	11.5	10
1980–1981	0.06	15	10
1970	0.07	16	22
1947–1948	0.18	32	101
1845	0.23	NA	77
1766–1768	0.4	NA	73
1693	0.3	NA	56
1636	0.18	NA	39
1597	0.29	NA	86
1510	0.32	NA	120
1389	0.15	NA	47
1341	0.18	NA	40
1300	0.5	NA	78
1222	0.04	NA	15
1206	0.4	NA	46
1158	0.33	NA	53
1104	2	36	> 230

NHESSD
2, 2463–2529, 2014

Table 2. Historical eruptions at Katla that produced tephra volumes > 0.1 km^3 (Thordarson and Larsen, 2007). Uncompacted volumes are presented either as *moderate* (> 0.1–0.5 km^3) or *large* (> 0.5 km^3).

Eruption year	Tephra volume
1918	Large
1755	Large
1721	Moderate
1660	Moderate
1625	Large
1500	Large
1416	Moderate
1357	Moderate
1262	Large
920	Moderate

NHESSD
2, 2463–2529, 2014

Table 3. Summary of ESP for all eruption scenarios.

Volcano	Reference eruption	Modelling strategy	Plume height (km a.s.l.)	Duration	Mass ($\times 10^{10}$ kg)	Md Φ	σΦ	Max Φ	Min Φ	Aggregation
Hekla	2000	ERS	6–16[a]	0.5–1 h[b]	6.9×10^{9}–6.9×10^{10}	–	–	−6	11	0.2–0.8[b]
	1947	ERS	16–30[a]	0.5–1 h[b]	6.9×10^{10}–3.5×10^{11}	−1–1 [c]	1–2[c]	−5	8	0.2–0.8[b]
Katla	Historical moderate/large[d]	LLERS	10–25[a]	1–4 days[b]	7×10^{11}–7×10^{12}	−1–1 [c]	1–2 [c]	−7	8	0.2–0.8 [b]
Eyjafjallajökull	2010	LLOES	2.5–7.8 [e]	40 days	–	–	–	−2	11	–
Askja	Askja C	OES	23	1 h	4.8×10^{11}	–	–	−6	6	0.2–0.8
	Askja D	OES	26	1.5 h	5.0×10^{11}	–	–	−10	6	0.2–0.8

[a] Logarithmic
[b] Uniform
[c] Gaussian
[d] Thordarson and Larsen (2007)
[e] IMO (Arason et al., 2011)

NHESSD
2, 2463–2529, 2014

Table 4. Critical thresholds for probability calculation.

Threshol	Unit	Potential impact	References
Ground load			
1	$kg\,m^{-2}$	Fluorine poisoning, electric flashover, closing of airports	Bebbington et al. (2008), Blong (1984), Thorarinsson and Sigvaldason (1972), Wilson et al. (2011)
10	$kg\,m^{-2}$	Impact on road traffic, damages on crops	Blong (1984), Wilson et al. (2011)
100	$kg\,m^{-2}$	Structural damages of weakest structures	Blong (1984), Marti et al. (2008), Spence et al. (2005)
Atmospheric concentration			
2	$mg\,m^{-3}$	Precautionary maintenance for jet engine	IVATF (2010)
Arrival time			
24	h	–	Guffanti et al. (2010)
Persistence time			
12	h	–	Ulfarsson and Unger (2011)

NHESSD
2, 2463–2529, 2014

Table 5. Probabilities, mean arrival time and mean persistence time for a concentration of $2\,mg\,m^{-3}$ for all FL combined above the selected airports shown in Fig. 1. NR: not reached.

Airport	Eruption scenario	Distance from vent (km)	Concentration probability (%)	Mean arrival time (h ± standard deviation)	Mean persistence time (h ± standard deviation)
Keflavik (BIKF)	Hekla 2000	141	17.0	3.8 ± 2.2	4.7 ± 3.6
	Hekla 1947	141	23.0	3.6 ± 3.2	7.4 ± 5.3
	Katla	178	41.1	24.9 ± 22.2	21.3 ± 15.2
	Askja 1875	303	16.8	9.2 ± 7.7	18.2 ± 12.4
Oslo Gardermoen (ENGM)	Hekla 2000	1635	0.0	NR	NR
	Hekla 1947	1635	0.5	17.7 ± 5.2	4.6 ± 1.9
	Katla	1603	6.7	45.1 ± 21.4	7 ± 5.4
	Askja 1875	1503	11.5	24.6 ± 12.1	6.9 ± 4.3
London Heathrow (EGLL)	Hekla 2000	1780	0.2	11.2 ± 3.2	2.9 ± 0.9
	Hekla 1947	1780	0.8	13.0 ± 3.2	3.4 ± 2.2
	Katla	1731	5.2	47.3 ± 24.4	9.8 ± 8.1
	Askja 1875	1767	8.5	22.6 ± 12.8	7.6 ± 4.4
Amsterdam Schipol (EHAM)	Hekla 2000	1909	0.1	15.3 ± 0	2.7 ± 0
	Hekla 1947	1909	0.5	15.9 ± 1.0	6.7 ± 3.6
	Katla	1862	7.3	48.6 ± 20.7	9.0 ± 7.1
	Askja 1875	1860	9.7	22.6 ± 7.2	8.0 ± 4.3
Copenhagen Kastrup (EKCH)	Hekla 2000	2000	0.0	NR	NR
	Hekla 1947	2000	0.3	20 ± 0.8	4.4 ± 1.6
	Katla	1938	5.0	50.9 ± 20.6	6.6 ± 4.8
	Askja 1875	1876	6.9	25.9 ± 9.3	6.0 ± 3.1
Paris Charles De Gaulle (LFPG)	Hekla 2000	2136	0.0	NR	NR
	Hekla 1947	2136	0.2	15.8 ± 0.4	3.4 ± 1.6
	Katla	2075	3.7	50 ± 25.8	9.1 ± 8.6
	Askja 1875	2106	8.1	27.6 ± 12.5	6.9 ± 3.7
Frankfurt (EDDF)	Hekla 2000	2223	0.0	NR	NR
	Hekla 1947	2223	0.3	18.7 ± 0.6	5.9 ± 1.5
	Katla	2175	5.2	47.9 ± 21.1	7.7 ± 5.3
	Askja 1875	2175	6.8	27.4 ± 11.7	6.6 ± 3.3

NHESSD
2, 2463–2529, 2014

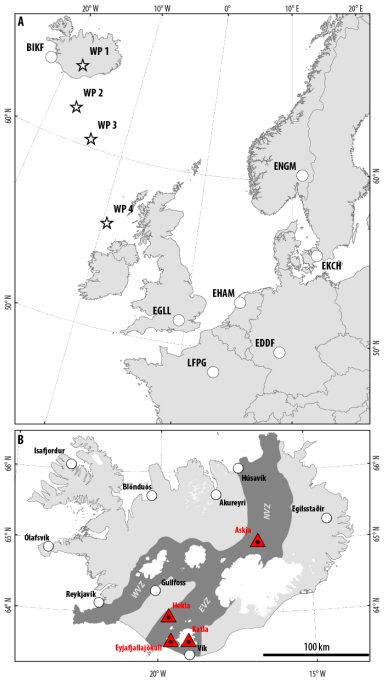

Fig. 1. Overview of the computational domains at large **(a)** and small **(b)** scales. The large scale map shows the locations of wind profiles (stars) used in Fig. 3 and the main airports (circles) of London Heathrow (EGLL), Paris Charles de Gaulle (LFPG), Amsterdam Schipol (EHAM), Frankfurt (EDDF), Oslo Gardemoen (ENGM), Copenhagen Kastrup (EKCH) and Keflavik (BIKF). The small scale maps shows the target volcanoes (red triangles) and the relevant volcanic zones for this study (WVZ: West Volcanic Zone; EVZ: East Volcanic zone; NVZ: North Volcanic Zone).

NHESSD
2, 2463–2529, 2014

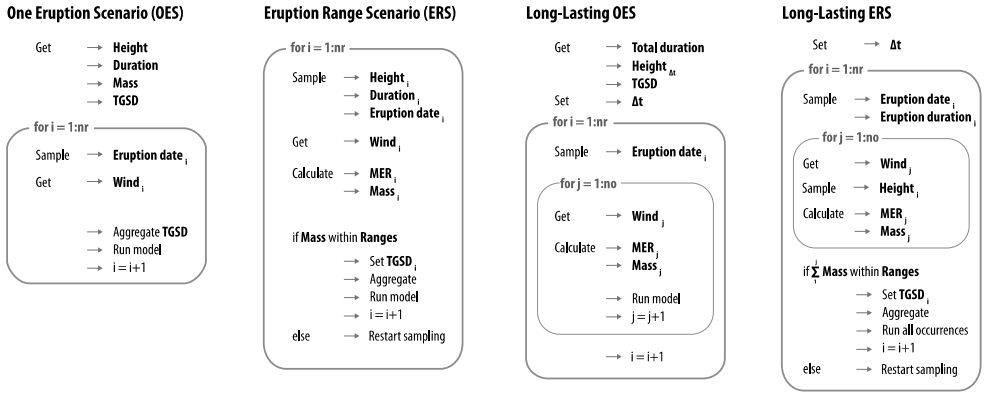

Fig. 2. Algorithms applied for the different eruption scenarios used in this study.

NHESSD
2, 2463–2529, 2014

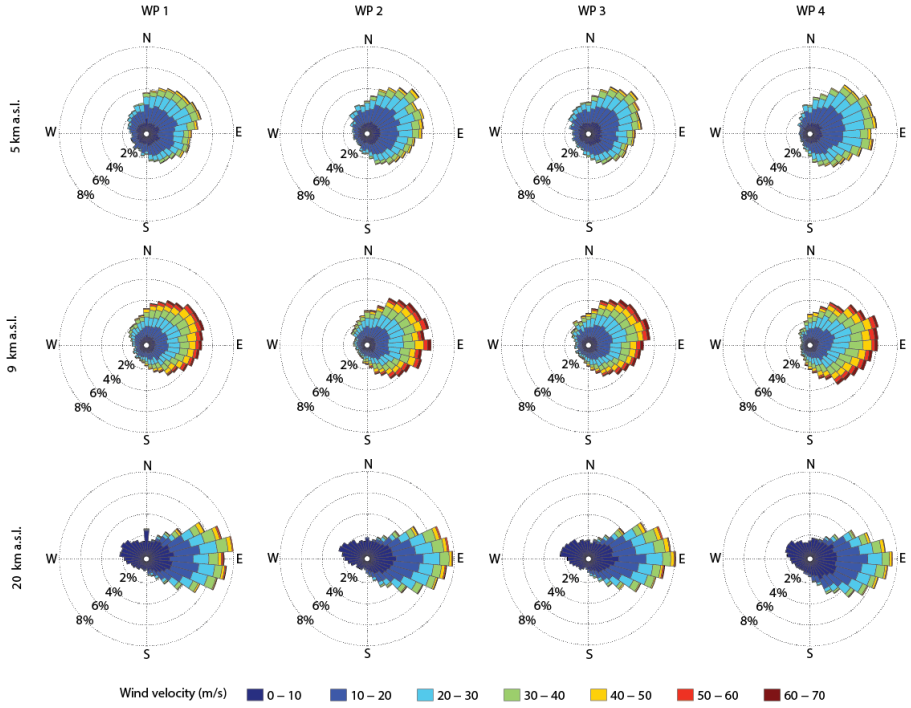

Fig. 3. Wind analysis at three atmospheric levels along a N–S section from Reykjavík to the UK (Fig. 1). WP 1 was obtained from the NCEP/NCAR Reanalysis database, WP 2–4 from the ERA-Interim Reanalysis database. These wind roses show the probability of the wind to blow in given directions and speed intervals.

NHESSD
2, 2463–2529, 2014

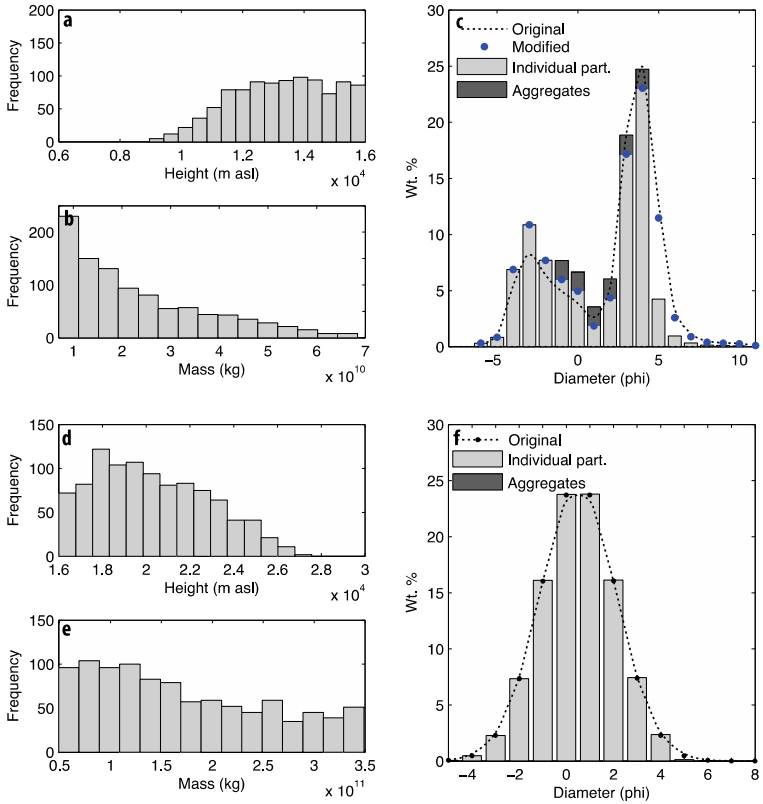

Fig. 4. ESP used for **(a–c)** the Hekla 2000-type and **(d–f)** the Hekla 1947-type scenarios (see Table 3 for details). **(a)** and **(d)**: plume height (m a.s.l.); **(b)** and **(d)**: erupted mass; **(c)** and **(f)**: total grainsize distribution. Histograms in **(c)** and **(f)** show both the fractions of individual particles (light grey) and aggregates (dark grey) generated based on the algorithm explained in the text; *original* indicates the original grainsize distribution obtained from sieving (i.e. not containing any aggregates).

NHESSD
2, 2463–2529, 2014

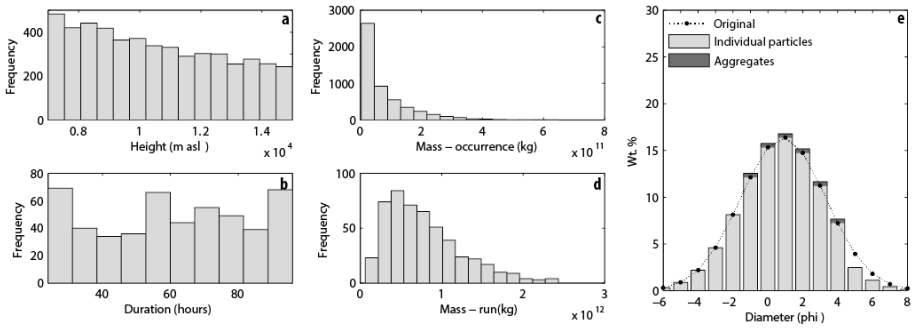

Fig. 5. ESP for the Katla LLERS; **(a)** plume heights considering all occurrences (i.e. all model runs); **(b)** eruption duration; **(c)** erupted masses considering all occurrences; **(d)** erupted masses considering single runs; **(e)** example of a TGSD of a single run. See caption of Fig. 4 for explanation of symbols.

NHESSD
2, 2463–2529, 2014

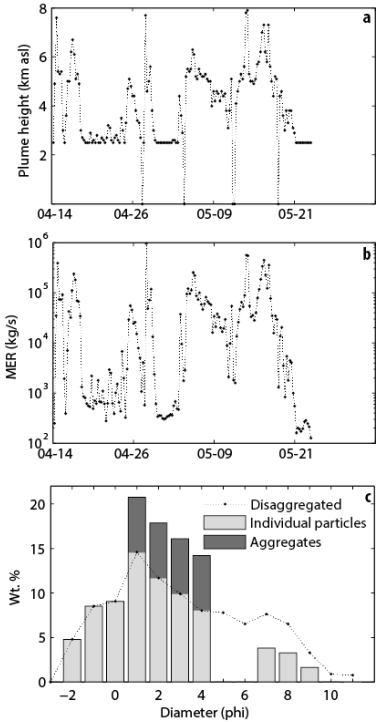

Fig. 6. ESP for the Eyjafjallajökull LLOES; **(a)** 6 h-interval measurements of plume height for the period 14 April–21 May 2010 (Arason et al., 2011); **(b)** corresponding MER for the same period based on wind conditions extracted from the NOAA Reanalysis database (Kalnay et al., 1996) and the method of Degruyter and Bonadonna (2012); **(c)** disaggregated and aggregated TGSD as inferred by Bonadonna et al. (2011). See caption of Fig. 4 for explanation of symbols.

NHESSD
2, 2463–2529, 2014

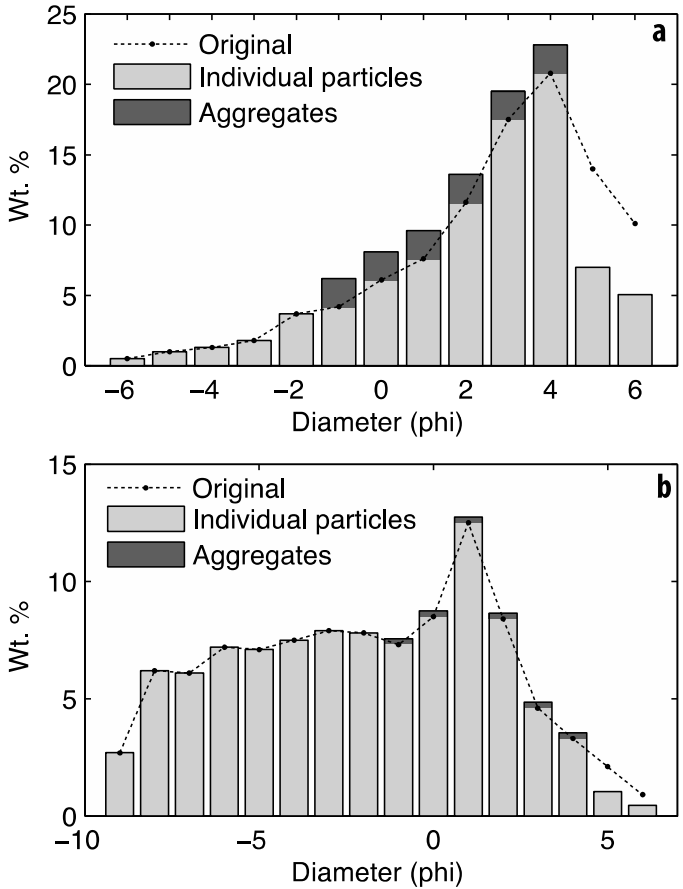

Fig. 7. Original and aggregated TGSD of the 1875 Askja eruption based on Sparks et al. (1981) for **(a)** the phreato-Plinian phase Askja C and **(b)** the dry Plinian phase Askja D. See caption of Fig. 4 for explanation of symbols.

NHESSD
2, 2463–2529, 2014

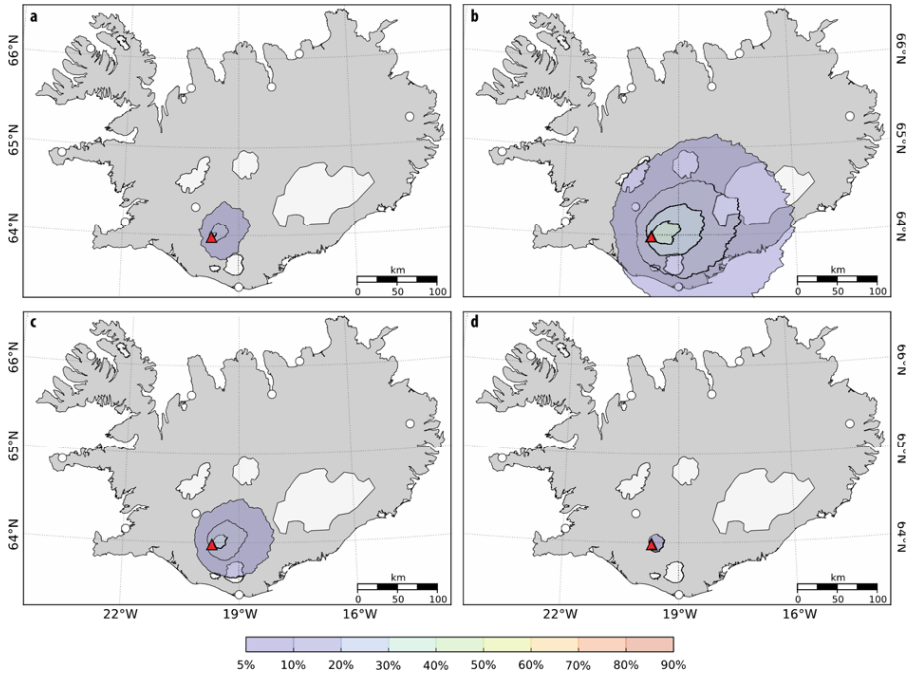

Fig. 8. Probability maps (%) for ground accumulation for an eruption at Hekla. **(a)** ERS for a 2000-type eruption, threshold of 1 kg m^{-2}; **(b)** ERS for a 1947-type eruption, threshold of 1 kg m^{-2}; **(c)** ERS for a 1947-type eruption, threshold of 10 kg m^{-2}; **(c)** ERS for a 1947-type eruption, threshold of 100 kg m^{-2}. Eruption parameters are summarized in Table 3 and Fig. 4.

NHESSD
2, 2463–2529, 2014

Hazard assessment for tephra dispersal from multiple Icelandic volcanoes

S. Biass et al.

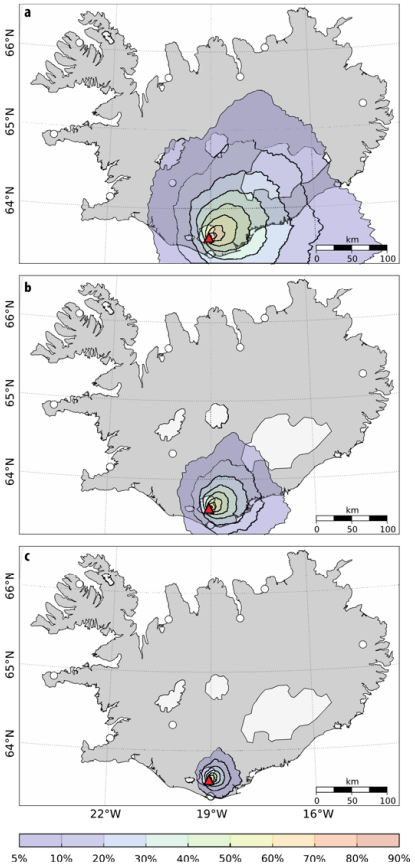

Fig. 9. Probability maps (%) for ground accumulation for a long-lasting eruption at Katla. **(a)** LLERS, threshold of 1 kg m^{-2}; **(b)** LLERS, threshold of 10 kg m^{-2}; **(c)** LLERS, threshold of 100 kg m^{-2}. Eruption parameters are summarized in Table 3 and Fig. 5.

NHESSD
2, 2463–2529, 2014

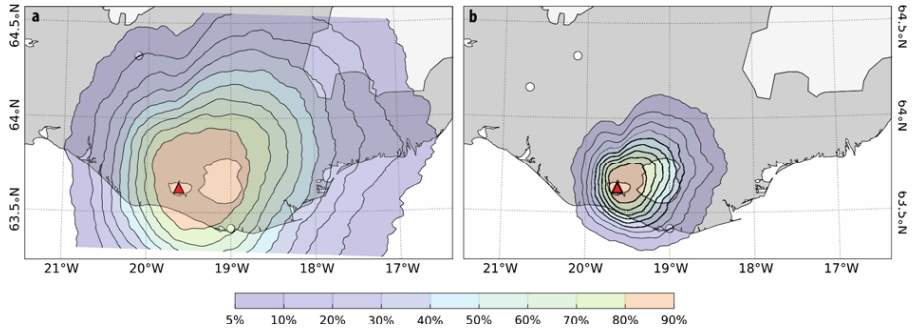

Fig. 10. Probability maps (%) for ground accumulation associated with a long-lasting 2010-type eruption of Eyjafjallajökull volcano. **(a)** LLOE, threshold of 1 kg m^{-2}; **(b)** LLOES, threshold of 10 kg m^{-2}. Eruption parameters are summarized in Table 3 and Fig. 6.

NHESSD
2, 2463–2529, 2014

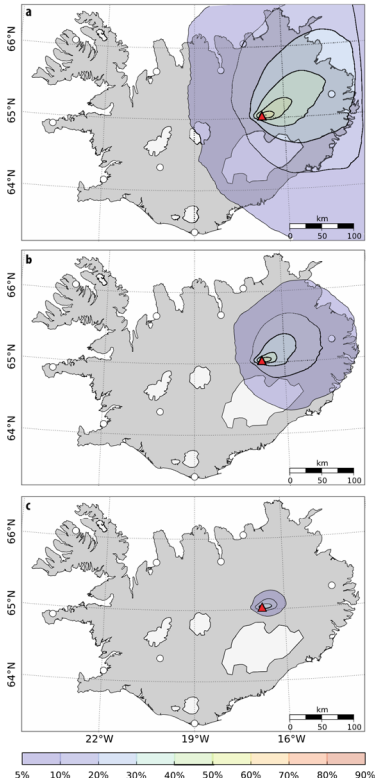

Fig. 11. Probability maps (%) for ground accumulation associated with a multi-phase 1875-type eruption at Askja volcano. **(a)** OES, threshold of 1 kg m^{-2}; **(b)** OES, threshold of 10 kg m^{-2}; **(c)** OES, threshold of 100 kg m^{-2}. Eruption parameters are summarized in Table 3 and Fig. 7.

NHESSD
2, 2463–2529, 2014

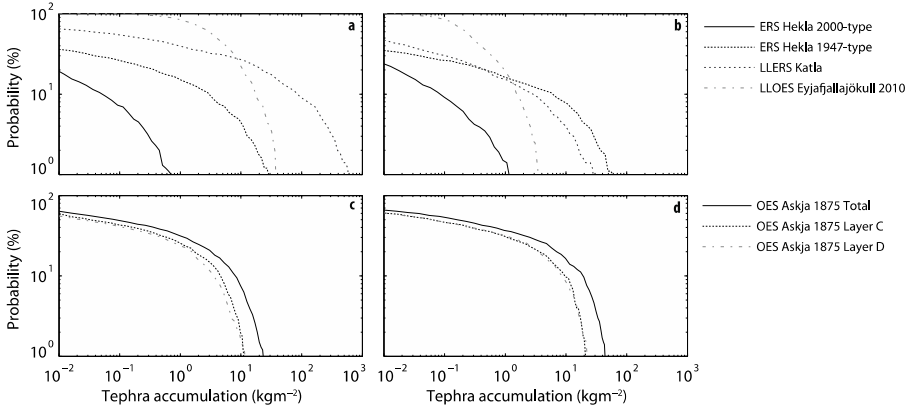

Fig. 12. Hazard curves for the locations of **(a)** Vík, **(b)** Gullfoss, **(c)** Akureyri and **(d)** Egilsstaðir (see locations in Fig. 1). Only relevant eruptions are shown at each location, i.e. ERS Hekla 2000- and 1947-type, LLERS of Katla and LLOES 2010-type of Eyjafjallajökull for Vík and Gullfoss and OES 1875-type of Askja (total eruption and individual phases) for Akureyri and Egilsstaðir.

NHESSD
2, 2463–2529, 2014

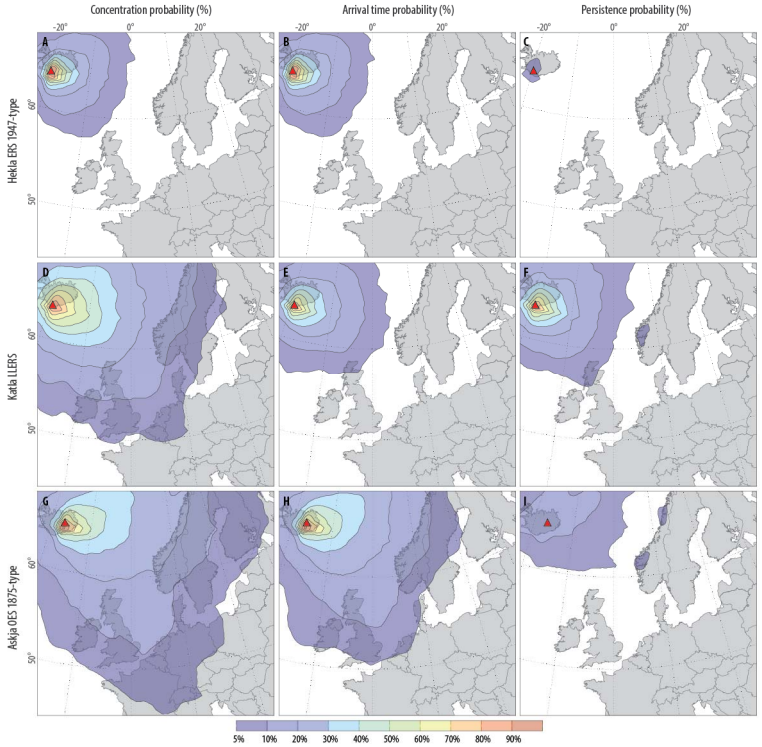

Fig. 13. Atmospheric dispersion of tephra for a threshold of 0.2 mg m^{-3} for all FL for the eruption scenarios of Hekla ERS 1947-type **(a, b, c)**, Katla LLERS **(d, e, f)** and Askja OES 1875-type **(g, h, i)**. Maps show **(a, d, g)** probability maps of exceeding a concentration of 2 mg m^{-3}, **(b, e, h)** probability maps of exceeding an arrival time of 24 h for a concentration of 2 mg m^{-3} and **(c, f, i)** probability maps of exceeding a persistence time of 12 h for a concentration of 2 mg m^{-3}. Probability maps for other thresholds and separate FL are available in the Supplement.

NHESSD
2, 2463–2529, 2014

Hazard assessment for tephra dispersal from multiple Icelandic volcanoes

S. Biass et al.

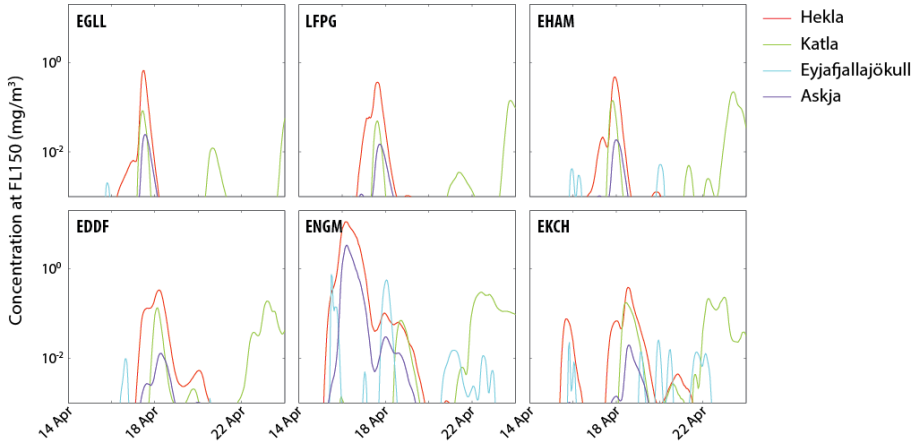

Fig. 14. Airborne concentration of ash at FL150 above the airports of London Heathrow (EGLL), Paris Charles de Gaulle (LFPG), Amsterdam Schipol (EHAM), Frankfurt (EDDF), Oslo Gardemoen (ENGM) and Copenhagen Kastrup (EKCH) resulting from the eruptions of Hekla 1947, Katla 1918, Eyjafjallajökull 2010 and Askja 1875. Each eruption was run for 10 days starting from 14 April 2010 using similar wind conditions that occurred during the Eyjafjallajökull 2010 eruption. Concentrations for other FL can be found in the Supplement.

NHESSD
2, 2463–2529, 2014